Hindawi
Geofluids
Volume 2020, Article ID 3568986, 24 pages
https://doi.org/10.1155/2020/3568986

Research Article

Paleofluid Fingerprint as an Independent Paleogeographic Correlation Tool: An Example from Pennsylvanian Sandstones and Neighboring Crystalline Rocks (Tisia Composite Terrane, S Hungary)

Krisztián Fintor and Andrea Varga

Department of Mineralogy, Geochemistry and Petrology, University of Szeged, H-6722, Hungary

Correspondence should be addressed to Andrea Varga; raucsikvarga@geo.u-szeged.hu

Received 28 October 2019; Accepted 1 February 2020; Published 17 March 2020

Guest Editor: Antonio Benedicto

In the basement areas of the southern Pannonian Basin, Central Europe (Tisia Composite Terrane, Hungary), Variscan blocks are essential components. The existing paleogeographic reconstructions, however, are often unclear and contradictory. This paper attempts to give a contribution for paleogeographic correlation of the Tisia using paleohydrological features (e.g., vein mineralization types, inclusion fluid composition and origin) of the Pennsylvanian continental succession and neighboring crystalline complexes. Vein-type mineralization in the studied samples dominantly forms blocky morphological types with inclusion-rich quartz and carbonate crystals. The evolution of hydrothermal mineralization and host rock alteration in the study area comprises three major stages. The first one is characterized by chloritization, epidotization, and sericitization of metamorphic rocks together with subsequent formation of Ca-Al-silicate and quartz-sulfide veins (clinopyroxene-dominant and epidote-dominant mineralization). The related fluid inclusion record consists of high-temperature and low-salinity aqueous inclusions, corresponding to a reduced retrograde-metamorphic fluid phase during the Late Westphalian (~310 Ma). The next mineralization stage can be related to a generally oxidized alkaline fluid phase with a cross-formational character (hematite-rich alkali feldspar-dominant and quartz-dolomite veins). High-salinity primary aqueous inclusions probably were originated from the Upper Permian playa fluids of the region. The parent fluid of the third event (ankerite-hosted inclusions) was derived from a more reductive and low-salinity environment and can represent a post-Variscan fluid system. Fluid evolution data presented in this paper support that the W Tisia (Mecsek–Villány area) belonged to the Central European Variscan belt close to the Bohemian Massif up to the Early Alpine orogenic phases. Its original position is presumably to the northeast from the Bohemian Massif at the Late Paleozoic, north to the Moravo-Silesian Zone. The presented paleofluid evolution refines previous models of the paleogeographic position of the Tisia and puts constraints on the evolution of the Variscan Europe.

1. Introduction

In the basement areas of the Pannonian Basin, Central Europe (Hungary), pre-Variscan and Variscan blocks are essential components [1–4]. Late Variscan age granitoids are known in the Tisia Composite Terrane or Tisza Megaunit (e.g., ca. 330–360 Ma, Mórágy Granite Complex) where locally marine Silurian and terrestrial Permo-Carboniferous (meta) sediments are also preserved (Figure 1). Based on its Variscan and early Alpine tectonostratigraphic characteristics, the Tisia was located at the margin of the European Plate prior to a rifting period in the Middle Jurassic [5–7]. The existing paleogeographic reconstructions, based on the correlation of the Paleozoic and Mesozoic facies belts in the Alpine–Carpathian domain, however, are contradictory (Figure 2). On the one hand, at the end of the Variscan cycle, the polymetamorphic complexes of the Tisia belonged to the southern part of the Moldanubian Zone, forming the

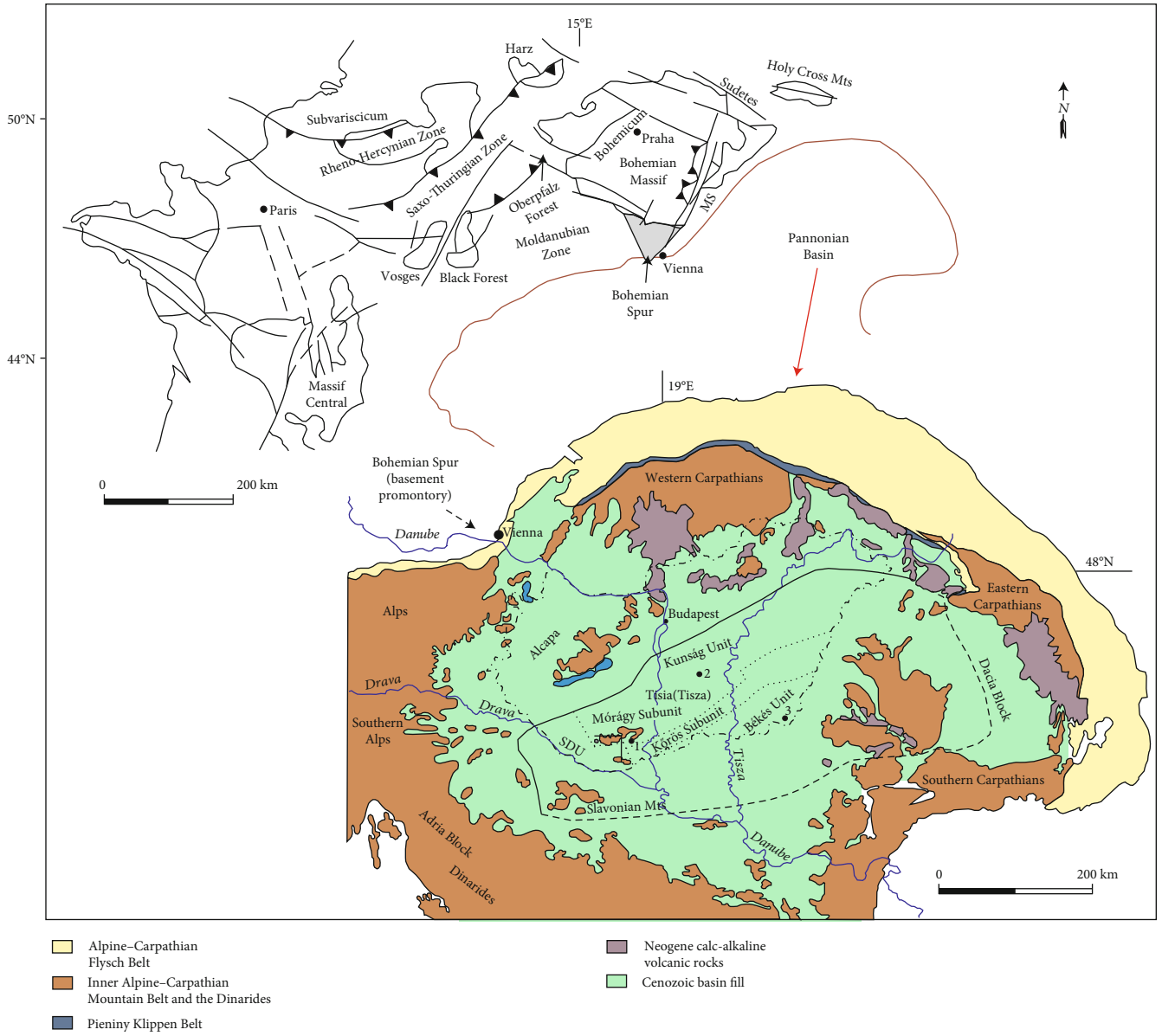

Figure 1: Regional geology. Simplified map of Variscan basement areas in W and Central Europe [1, 8] and geologic framework of the Carpathian–Pannonian area [1, 4]. Late Variscan age granitoids known in the Hungarian part of the Tisia are also indicated [2]. 1: Mecsek Mountains (Mórágy Complex), monzonite; 2: Danube–Tisza Interfluve, Kecskemét basement area, monzonite; 3: Battonya basement area, tonalite. Box indicates area studied in detail (see Figure 3(a)). MS: Moravo–Silesian (Brunovistulian) Zone; ALCAPA: Alpine–West Carpathian–Pannonian Block; SDU: Slavonia–Drava Unit.

European margin of the Paleo-Tethys [2, 3, 5]. Position of the Tisia can be determined east to the Bohemian Massif and to the Western Carpathians (Figure 2(a)).

On the other hand, the Bohemian Massif can project below the Eastern Alps and the Vienna Basin as a major basement promontory referred to as the Bohemian Spur [9, 11]. According to this concept, the conjugate upper margin can be found in the northern edge of the Moesian Platform (Romania and Bulgaria) which is a large microplate between the Southern Carpathians and the Balkans [12]. Therefore, its pre-Middle Jurassic reconstruction between the Bohemian Spur and the Teisseyre-Tornquist Zone leaves no space for the Tisia in this segment of the European margin (Figures 1 and 2(b)). Consequently, the original paleogeographic position of the Tisia on the European southern margin had to be to the west of the Bohemian Spur, having the structural characteristics of syn-rift development during the latest Triassic and Early Jurassic (e.g., pronounced extensional half-grabens with the characteristic Gresten facies siliciclastic basin fill) [9, 13]. This scenario was recently reinforced [14], suggesting a connection of the Tisia to the southern and/or southwestern part of the Bohemian Massif.

If the assumption that the Tisia was an integrated part of the Moldanubian Zone up to the latest Triassic is correct, at least some lithostratigraphic units from both areas

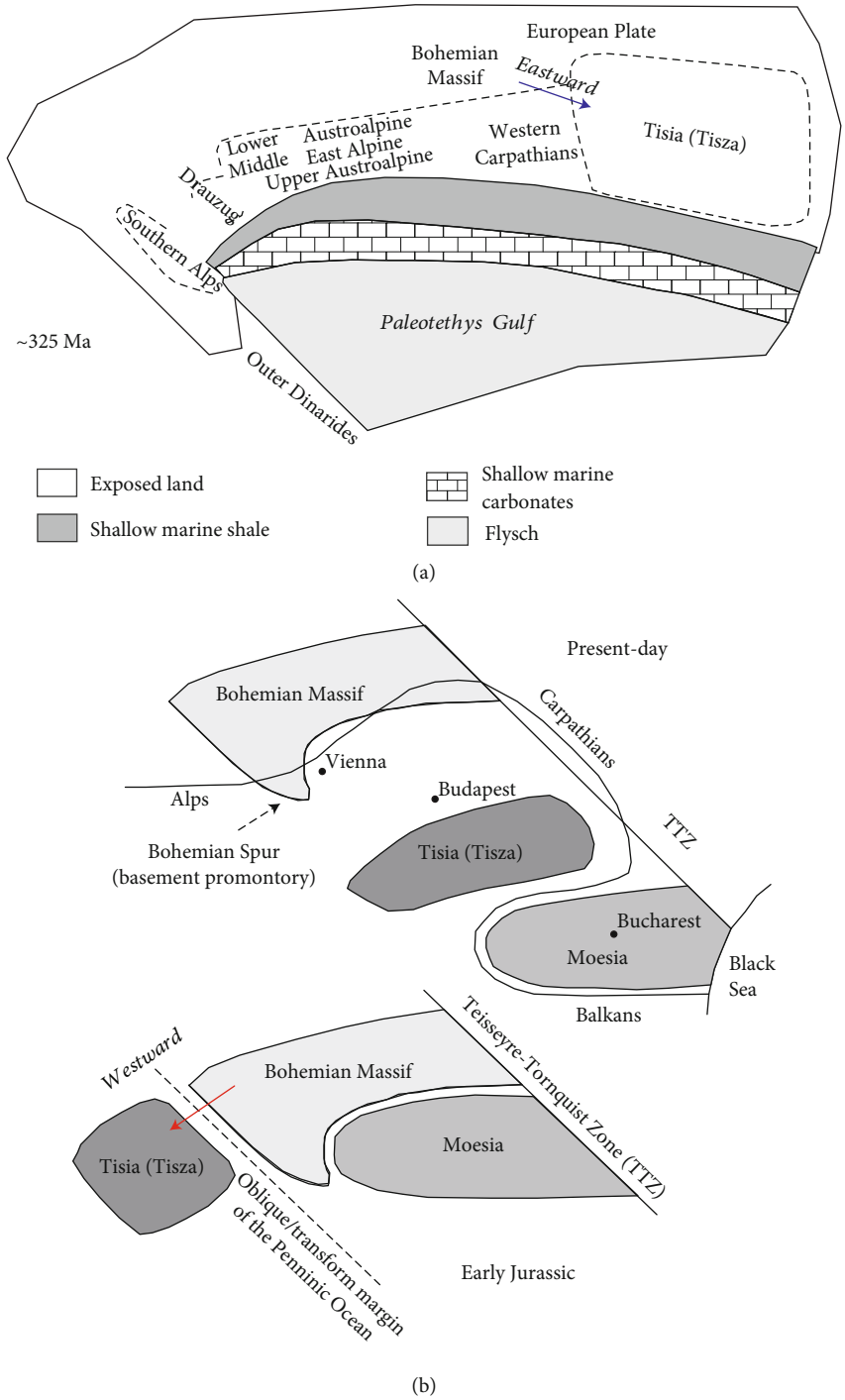

Figure 2: Speculative paleogeographic position of the Tisia. (a) Paleogeographic reconstruction for the Early Carboniferous [5]. (b) Position of the Tisia for the Early Jurassic [9]. The present-day outline of the Tisia is the end-result of severe continental E–W extension during the Miocene and equally important Eo-Alpine N–S shortening during the Cretaceous [10]. Thus, a more likely pre-Albian map-view outline of the Tisia should have an isometric shape [9].

should be characterized by similar Late Variscan and post-Variscan large-scale hydrothermal events and host rock alteration styles. Veins are common features in rocks and extremely useful structures to determine pressure-temperature range, fluid composition, and fluid origin during their formation [15]. This paper attempts to give a contribution for paleogeographic correlation of the Tisia Composite Terrane using paleofluid features of the Pennsylvanian (Upper Carboniferous) continental succession, Téseny Formation, S Hungary. In addition, the results from previous vein petrological and geochemical studies of the Téseny Formation and neighboring crystalline complexes in the study area [16–25] have also been integrated into this paper.

A multidisciplinary approach including vein petrography, cathodoluminescence (CL) and Raman microspectroscopy, X-ray fluorescence analyses, stable O and C isotope analyses, and fluid inclusion petrography and microthermometry was applied to unravel the tectono-sedimentary record of the Téseny siliciclastic deposits in the Slavonia–Drava Unit (Figure 1). The paleofluid evolution presented in this article refines previous models of the tectonic history of the Tisia and puts constraints on the evolution of the Variscan Europe.

2. Geological Setting

The Tisia Composite Terrane, corresponding to a structural mega-unit, forms the basement of the southern Pannonian Basin [4, 6, 7]. Within the crystalline basement, three terranes have been distinguished: (1) Slavonia–Drava Unit, which can be subdivided into the Babócsa and Baksa Complexes (Subunits); (2) Kunság Unit, including Variscan granitoids of the Mórágy Complex; and (3) Békés Unit [4]. The study area includes the western Mecsek Mountains, which are parts of the Kunság Unit (Mórágy Subunit), and the western flank of the Villány Mountains which is a part of the Slavonia–Drava Unit (Figures 1 and 3(a)). The crystalline complexes and the overlying Paleozoic and Mesozoic sequences show heterogeneous lithological and metamorphic characteristics, indicating various phases of geologic evolution [4, 7]. The oldest Paleozoic rocks are the late Early Silurian Szalatnak Slate deposits (Szalatnak Unit) related to a marine clastic sedimentation. In the Pennsylvanian, a molasse-type siliciclastic and, locally, coal-bearing sequence called Téseny Sandstone Formation was deposited in a foreland basin. In the Permian, continental red beds together with volcanosediments characterized the development of the study area [1, 4, 24, 26–28].

The nonmetamorphic (locally anchimetamorphic) Téseny Formation is interpreted as a fluvial system deposit. It unconformably overlies the Babócsa and Baksa metamorphic basement complexes and has a maximum thickness of 1500 m, occurring subsurface in the area between the Mecsek and Villány Mountains (Figure 3(a)). It is composed of conglomerate, sandstone, and siltstone; in addition, shale and coal seams also occur. These rocks contain a Namurian–Westphalian flora and Westphalian palynomorphs [24, 25, 29–31].

Téseny rocks are known from numerous shallow wells in the western flank of the Villány Mountains (Figure 3), for example, in wells Téseny–2 (T–2) to Téseny–7 (T–7). Additionally, it was also penetrated in deep boreholes Bogádmindszent–1 (Bm–1), Diósviszló–1 (Dv–3), and Siklósbodony–1 (Sb–1). Lithologically, the Téseny Sandstone samples are poorly to moderately sorted lithic-feldspathic wacke to arenite and arkose. They are composed of variable amounts of quartz, plagioclase, K-feldspar, micas, chlorite, clays, Fe oxides, and lithic grains such as quartz-rich metamorphic, acidic-intermediate volcanic, granitoid, and siliciclastic rock fragments [20–24]. The poorly to moderately sorted polymictic Téseny conglomerate samples are characterized by metamorphic, sedimentary, and acidic-intermediate volcanic rock clasts [21, 24, 29–31].

In the joints of the Pennsylvanian rocks from the wells near the village of Téseny, two fracture filling types were previously distinguished [29]: (1) an older vein-type carbonate-feldspar mineralization, which comprises kidney-shaped siderite, K-feldspar, and chlorite and (2) a younger pure quartz infilling. Furthermore, mm-to-cm-thick veins ("aplite dykes") were also described in the boreholes Bm–1 and Sb–1 which comprise quartz, dolomite, K-feldspar, and chlorite [31]. Petrographic features of some Téseny Sandstone samples reflect extensive hydrothermal alteration with concomitant pyritization. Alteration styles that accompany this disseminated sulfide mineralization comprise carbonatization, silicification, chloritization, and sericitization of the host rock [22–25].

3. Materials and Methods

For petrographic analysis of the Pennsylvanian Téseny rocks, Mining and Geological Survey of Hungary provided thin section collection from borehole Bm–1 (date of drilling: 1968) at depths of 848.9–1350.0 m below surface. Covered thin sections ($n = 373$) were studied by polarized light microscopy. The petrographic characterization of the observed veins (1 cm wide maximum), occurring in 27 thin sections, is based on papers by Bons [15, 32]. Additionally, thin section collection ($n = 11$) of the Eötvös Loránd University, Budapest, from the wells near the village of Téseny (date of drillings: 1967) was also used for petrographic analysis. After that, a total of 11 core samples from the boreholes Bm–1, T–3, T–5, T–6, and T–7 were newly collected for this study. Detailed vein petrographic descriptions using CL microscopy, X-ray fluorescence analysis, and fluid inclusion study were conducted on representative thin sections (quartz and quartz-carbonate vein types). Vein sample locations ($n = 40$) are shown in Figure 3(b). Conventional mineral abbreviations have been used during the whole manuscript [33].

Cathodoluminescence (CL) studies were carried out by a Reliotron cold cathode luminoscope operating at 8 kV and 0.7 mA at the host department. Photomicrographs were made using an Olympus DP73 camera and the exposure times varied between 1 and 3 min.

X-ray element maps of representative areas of selected samples and single point analyses were made in order to monitor compositional variations of the minerals using a Horiba Jobin Yvon XGT 5000 X-ray fluorescence spectrometer at the host department. In the case of carbonates, Ca, Mg, Fe, and Mn were measured while Pb, Bi, Zn, Cu, Fe, As, Sb, Sn, Ag, Se, Te, Au, Ga, and Cd were analyzed for galena. Standardization was made by natural internal standards. Beam diameter was 100 μm and acceleration voltage was 30 kV during element mapping. Operating conditions of point analyses for carbonates and galena were 30 kV accelerating voltage and beam diameter 100 μm and 50 kV voltage with beam diameter 100 μm, respectively.

Fluid inclusions were studied in 75–150 μm double-polished thick sections prepared from the vein materials at the host department. A low speed sawing machine was used

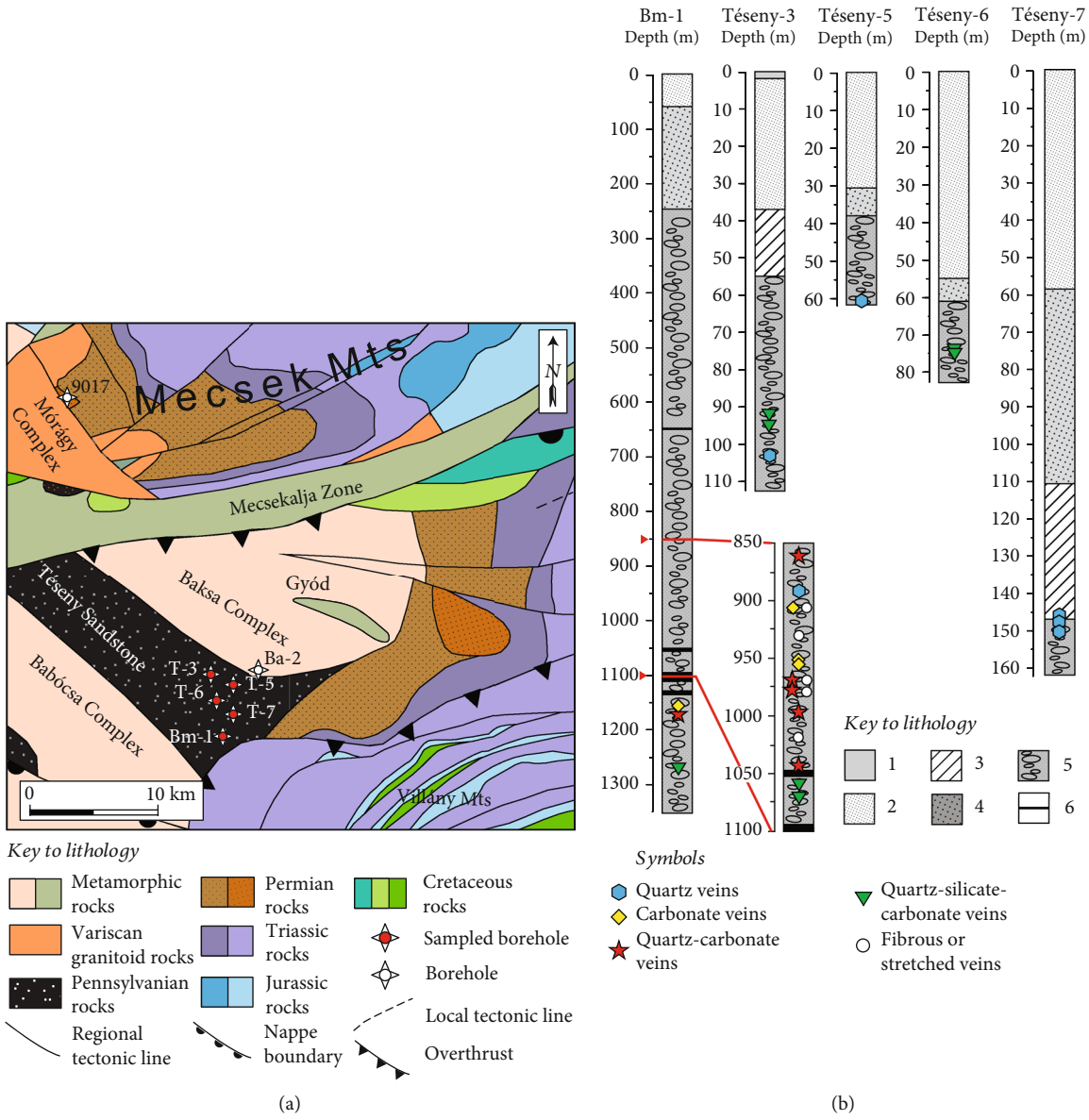

Figure 3: Local geology. (a) Generalized geologic map of the Mecsek–Villány area, S Hungary, showing the pre-Neogene basement formations [4]. (b) Schematic lithologic logs of the studied boreholes, showing the positions of the investigated cores within the hole. Bm-1: Bogádmindszent–1. Key to lithology: 1: Holocene soil; 2: Pleistocene sand, loess, and red clay; 3: Upper Miocene sand, clay, and/or marl, lower part; 4: Upper Miocene sand, clay, and bentonite, upper part; 5: Pennsylvanian (Upper Carboniferous) sandstone and conglomerate; 6: coal seams.

to cut the samples in order to avoid changes in the volumes of the fluid inclusions. Microthermometric measurements were carried out with a Linkam THMSG 600 heating-freezing stage operating over a temperature range from −190 to +600°C. Synthetic fluid inclusions were used to calibrate at −56.6, 0.0, and +374.0°C. The accuracy of the data is approximately ±0.2°C under freezing and ±0.5°C under heating conditions. An LMPlanFI 100x objective lens (Olympus) was used to analyze the inclusions. The measurements of inclusions trapped in quartz began with freezing, while in the case of carbonate, the heating experiments were carried out first. In the latter case, inclusions can suffer permanent deformation during the freezing experiment [34]. The cycling method [34] was used to determine the last ice melting temperature of fluids trapped in calcite. Determinations of volume fractions of vapor bubbles (φ_{vap}) were obtained from area analysis in a two-dimensional projection of fluid inclusions. Terms and symbols are used after Diamond [35].

Thermodynamic model to derive the behavior of high-salinity H_2O-salt system with complex composition does not exist yet [36]. Failing a model, the salinities are calculated based on the equivalent mass% principle in the H_2O–NaCl binary and H_2O–NaCl–$CaCl_2$ ternary model systems. Salinity calculations are based on T_m (ice) and T_m (Hh) data of fluid inclusions using AqSo-Vir software by Bakker [37], corresponding to a numerical model [38]. Program module

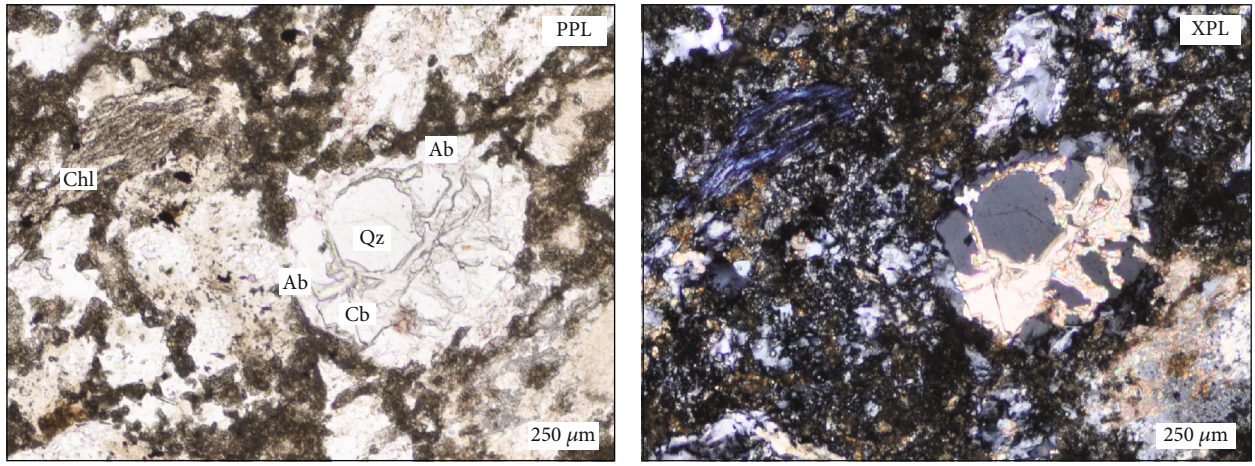

(a) (b)

FIGURE 4: Hydrothermal alteration of siliciclastic host rocks (borehole Bm–1, 1062.3 m). Note: dissolution of quartz (Qz) from the framework grains followed by albitization (Ab), pervasive carbonatization (Cb), and chloritization (Chl). Abbreviations: PPL: plane-polarized light; XPL: crossed polars.

BULK from program package FLUIDS [36] was used to determine the main physical parameters such as homogenization pressure (p_h), molar volume (V_m), and liquid to vapor ratio (φ_{vap}) of fluid inclusions. This program uses equations of state (EoS) of Zhang and Frantz [39] in the case of bulk fluid inclusion and EoS of Krumgalz et al. [40] in the case of aqueous fluids.

Raman microscopic analysis of fluid inclusions was carried out at the Department of Mineralogy and Petrology of Montanuniversität Leoben using a Jobin Yvon LABRAM confocal Raman microspectroscope which works with a frequency-doubled Nd-YAG laser of 100 mW capacity. Irradiations were made by using a laser light with 532.2 nm (green) wavelength in the case of each sample. The instrument is characterized by 4 cm^{-1} spectral- and few μm^3 spatial resolutions. The calibration of the spectrometer was made by using synthetic silicon chip, polyethylene, calcite, and natural diamond crystal. Recording time was 150 sec in the case of each spectrum with 30 sec accumulation periods. Raman spectra of salt hydrates can be found in the range of 3000–3700 cm^{-1} with a most important peaks around 3400 cm^{-1} [41, 42]. During Raman spectroscopy-assisted microthermometry, the Linkam THMSG 600 heating-freezing stage was mounted on the Raman spectrometer. In order to make accurate identification of ice and salt hydrates, spectra were recorded at temperature condition lower than −170°C. This method is applicable with great efficiency to determine last melting temperature of salt hydrates and to distinguish the different types of salt hydrates from ice and each other.

Stable isotope analyses for seven representative carbonate samples were made using a Finnigan delta plus XP mass spectrometer at the Research Centre for Astronomy and Earth Sciences of the Hungarian Academy of Sciences, Budapest. The sampling was done by microdrilling of crack filling carbonate, obtaining 0.1–0.3 mg powder. Each sample was reacted with purified phosphoric acid, producing CO_2 gas which was analyzed by the mass spectrometer. The isotopic compositions $\delta^{13}C$ (V-PDB) and $\delta^{18}O$ (V-SMOW) of each sample are averages of replicate analyses. Precision of the measurements was ±0.1–0.2‰ in cases of $\delta^{13}C$ and $\delta^{18}O$. The ^{13}C and ^{18}O isotope results are reported in the standard δ notation of the difference in isotope ratio between the sample and a standard expressed in per mil (‰), where $\delta = [(R_{sample}/R_{standard}) - 1] * 1000$.

4. Results

4.1. Vein Classification and Petrography. Based on their geometric, textural, and mineralogical characteristics, the observed veins can be subdivided into four main groups: (1) blocky, (2) fibrous, (3) stretched, and (4) polytextured veins. Additionally, four subtypes of blocky veins can be distinguished, based on dominant mineral phases. Hydrothermal alteration of the siliciclastic host rock is rare; although, adjacent to some quartz-silicate-carbonate blocky veins, millimeter–submillimeter thick zones of feldspar alteration, carbonatization, and chloritization are present (Figure 4).

4.1.1. Blocky Veins

(1) Quartz Veins. This subtype contains almost exclusively quartz as a fracture filling mineral. Thickness of the veins is in a range of ~0.2–5 mm. They are closely parallel or at 10–30° angle to the long axis of the drill core. Most of the quartz veins are filled almost entirely euhedral and/or subhedral quartz crystals which are generally deposited directly to the vein walls. At some places, however, vein walls are coated by microcrystalline iron oxide/hydroxide (goethite; <1 mm in thickness) preceding quartz mineralization. Some of the quartz veins show elongate blocky texture where the *c*-axis of each crystal is close to perpendicular to the vein wall and tiny open cavities are observable among them frequently. Most of the quartz crystals are exhibiting well-developed growth zonation patterns indicated by fluid inclusion bands.

Additionally, faintly brown-luminescent adularia crystals subordinately occur either as replacement and/or overgrowth on blue-luminescent detrital K-feldspar grains of the sandstone wall rock or as a fracture filling mineral among the quartz crystals (Figure S1).

(2) Carbonate Veins. This subtype contains almost exclusively carbonate (mainly dolomite) fracture filling minerals. Thickness of these veins is in a range of ~0.05–1 mm. Sparry dolomite crystals have curved crystal boundaries and undulose (sweeping) extinction (Figure S1).

(3) Quartz-Carbonate Veins. This subtype can be found only in the drill core samples from the borehole Bm–1 where these veins occur frequently. Their thickness is in a range of ~0.01–1 cm and they are at 30–35° angle with the long axis of the core. The quartz-carbonate veins are composed of symmetrical fracture infilling. Within the veins, quartz is deposited directly on the walls as euhedral crystals followed by a white colored sparry carbonate phase (mainly dolomite). This latter phase shows bulky habit and, in thin section, is characterized by a hypidiomorphic appearance with curved crystal boundaries (Figure S2).

Quartz crystals show growth zonation that is marked by fluid inclusion assemblages, while CL microscopy reveals a more detailed internal growth zonation pattern. Cores of the carbonate crystals show significant turbidity owned to fluid inclusion clusters. Their rims are, however, clear so they are free from fluid inclusions. Majority of the carbonate crystals display undulose extinction but do not show any deformation twins (Figure S2). Raman measurements indicate that these crystals are dolomites (characteristic bands: ~1098, ~300, and ~176 cm^{-1}; http://rruff.info/ [43, 44]). Millimeter-sized blocky crystals of galena occur sporadically in the pore space among dolomite crystals. The dolomite and galena assemblage is followed by a carbonate phase with growth zonation pattern marked by fluid inclusion bands. This latter carbonate phase is ankerite (characteristic bands: ~1093, ~289, and ~172 cm^{-1}; http://rruff.info/ [43, 44]).

Using CL microscopy, the rhombohedral dolomite crystals with curved faces are nonluminescent while their very thin (<10 μm) clear rims have a characteristic red luminescence. The following ankerite shows fine-scale oscillatory zonation containing thin red- and nonluminescent bands. Tiny calcite crystals (~5–20 μm) with a bright orange luminescence can be found frequently as solid inclusions in this oscillatory zoned phase (Figure S2).

(4) Quartz-Silicate-Carbonate Veins. This subtype can be found in several investigated boreholes but not occurs so frequently than the abovementioned blocky ones. This subtype contains dominantly euhedral quartz crystals and sparry habit alkali feldspars where the latter show turbid internal texture caused by minute hematite inclusions. More or less amount of chlorite±kaolin minerals, botryoidal calcite, and sulfide minerals (mainly pyrite) with a minor amount of epidote and Ti-oxides also occur in these veins (Figure S2). In a single sample from the lowermost part of the Pennsylvanian section (borehole Bm–1 1062.1 m), chlorite and/or pyrite are accompanied by euhedral monazite and/or xenotime crystals (Figure S3).

4.1.2. Fibrous Veins. Fibrous veins appear only in subordinate amounts and their thickness is lesser than 1 mm. They are emplaced parallel or at very small angle (<20°) to sedimentary bedding. Elongated fibrous crystals are parallel with each other and perpendicular to the vein plane. The observed internal microstructure indicates antitaxial growth morphology. Two subtypes can be distinguished among them, one with solid inclusion trails which are parallel with the vein walls. This subtype occasionally contains quartz beyond the dominant carbonate fracture filling mineral. The other subtype is made by carbonate and frequently contains sinusoidal solid inclusion bands (Figure S4).

4.1.3. Stretched Veins. Stretched veins occur in subordinate amounts and contain dominantly stretched crystals of quartz together with minor amounts of chlorite or carbonates (Figure S4). The thickness of these veins is in a range of 0.2–1 mm.

4.1.4. Polytextured Vein. Polytextured vein is the rarest vein type in the investigated area (only a single studied sample). It contains a fibrous carbonate on the vein wall that is followed by a blocky textured carbonate in the middle of the vein (Figure S4).

4.2. Mineral Chemistry. In order to reveal the element distribution in the carbonate phases of quartz-carbonate veins, X-ray element maps have been carried out (Figure 5). The results indicate that dolomite is chemically homogeneous. On the other hand, two chemically distinct parts can be observed in ankerite. At the contact with dolomite, a thick band (50–200 μm) is enriched in Mn (Ank_{Mn}) while other parts do not show Mn enrichment only the higher iron content is typical for ankerite (Ank_{Fe}). Point analyses of dolomite indicate some iron substitution (Table S1). Their $FeCO_3$ content varies between 8 and 10 mass% while $MnCO_3$ content is <2 mass%. Composition of Ank_{Mn} shows 14–18 mass% $FeCO_3$ and 5–8 mass% $MnCO_3$ concentration, while $MnCO_3$ content of Ank_{Fe} shows 2–5 mass% and their $FeCO_3$ content varies in a wide range of 15–23 mass%.

Composition of galena differs a little bit from the stochiometric composition (~86 mass% Pb and ~14 mass% S, respectively). Its Pb content varies between 83 and 89 mass% while S content is in a range of 8–15 mass% with a relatively high Bi (0.5–1.4 mass%) content (Table S2). The analyzed galena is relatively rich in Ag (2200–4300 ppm), Se (1400–5100 ppm), and Sn (1100–2900 ppm).

4.3. Stable Isotopes. A total of seven carbonate samples from quartz-carbonate veins were selected for stable isotope analyses (Table S3). The $\delta^{13}C$ (V-PDB) and $\delta^{18}O$ (V-PDB) values for dolomite vary from −6.15 to −5.77‰ and from −16.63 to −16.21‰, respectively. The studied ankerite samples display $\delta^{13}C$ (V-PDB) values from −5.64 to −5.39‰ and $\delta^{18}O$ (V-PDB) values from −16.09 to −14.93‰.

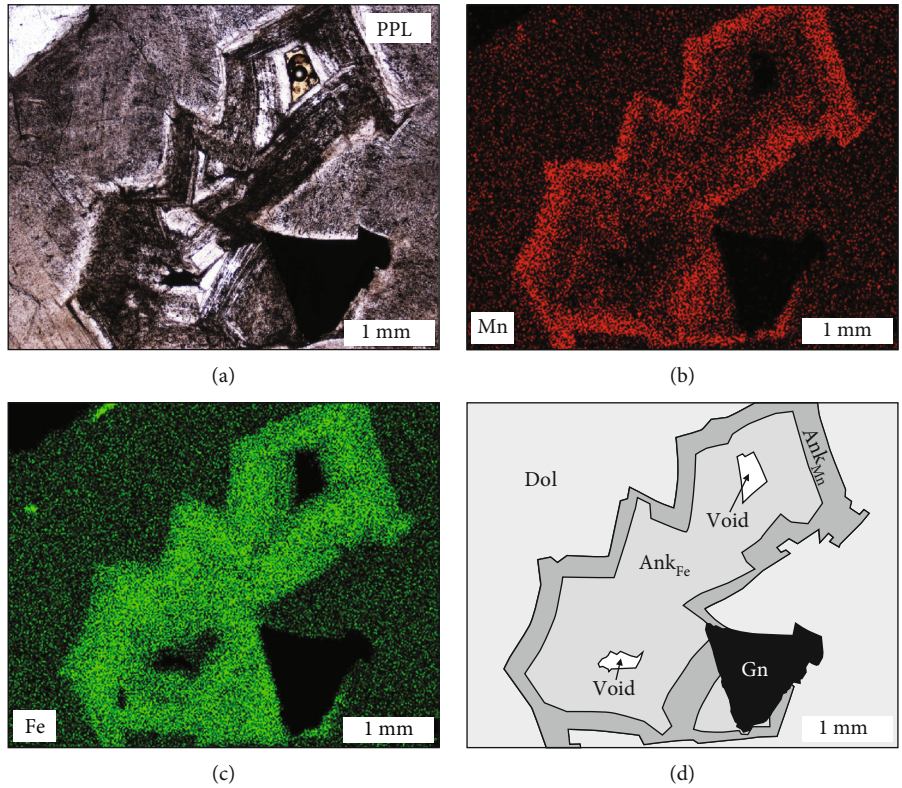

Figure 5: X-ray element maps of carbonate phases of quartz-carbonate vein type (borehole Bm–1, 875.0 m). (a) Different carbonate phases together with galena in the quartz-carbonate vein type. (b, c) Distribution of intensity of Fe Kα line (green color) and Mn Kα line (red color) of ED spectra of the same area, respectively. (d) Summary outline about the textural distribution of different carbonate phases based upon petrographic, phase analytical (Raman), and EDS mapping information. Abbreviations: Dol: dolomite; Ank: ankerite; Gn: galena; PPL: plane-polarized light.

Table 1: Petrographic characteristics and microthermometric data of the studied primary fluid inclusions.

Mineral phases		T_h (°C)	T_i (°C)	T_m(ice) (°C)	T_m (Hh) (°C)	Salinity H_2O-NaCl-$CaCl_2$		H_2O-NaCl
Quartz vein						NaCl (mass%)	$CaCl_2$ (mass%)	NaCl (mass%)
Quartz	QP1	88 to 145	−53.7 to −47.8	−26.0 to −21.0	−22.0 to −2.8	15.2 to 22.4	2.6 to 11.7	—
	QP2	63 to 89	−53.4 to −49.7	−25.3 to −23.1	−13.0 to −3.4	16.0 to 19.4	6.6 to 10.6	—
	QP3	50 to 77	−56.2 to −50.7	−27.0 to −23.0	−17.0 to −5.2	15.0 to 20.7	5.3 to 11.8	—
Quartz-carbonate vein								
Quartz	QCP1	54 to 153	−55.2 to −52.4	−25.4 to −22.8	−16.0 to −1.6	16.4 to 21.2	4.8 to 10.6	—
	QCP2	46 to 82	−52.7 to −47.6	−25.2 to −22.8	−14.0 to −6.7	16.2 to 20.4	5.3 to 10.3	—
	QCP3	42 to 78	−56.3 to −47.3	−28.0 to −23.8	−25.0 to −6.5	10.3 to 19.1	7.2 to 15.6	—
	QCP4	47 to 74	−54.1 to −47.7	−25.0 to −21.7	−17.4 to −9.8	15.8 to 23.6	1.6 to 10.1	—
Dolomite	DP1	127 to 167	−57.5 to −48.5	−28.6 to −25.5	—	—	22.8 to 24.2	—
Ankerite	AP1	61 to 109	—	−2.5 to −1.6	—	—	—	2.7 to 4.6

Abbreviations: T_h: temperature of homogenization; T_i: temperature of initial melting; T_m (ice): temperature of final melting of ice; T_m (Hh): temperature of final melting of hydrohalite; QP: primary fluid inclusions trapped in quartz from quartz veins; QCP: primary fluid inclusions trapped in quartz from quartz-carbonate veins; DP: primary inclusions trapped in dolomite; AP: primary inclusions trapped in ankerite.

4.4. Fluid Inclusions. Petrographic characteristics and microthermometric data of the studied fluid inclusion assemblages are summarized in Table 1. The raw data can be found in the Supplementary Materials (Table S4).

4.4.1. Quartz Veins. In the well-grown quartz crystals, primary fluid inclusions can be distinguished due to their location along growing zones of the host crystal. In the euhedral quartz, three primary fluid inclusion assemblages (FIAs:

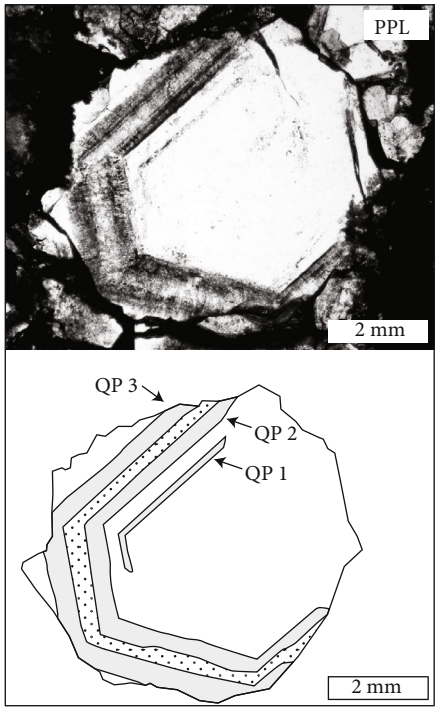

Figure 6: Photomicrograph and sketch about the arrangement of primary fluid inclusion assemblages (QP1 to QP3) in a quartz single crystal from a quartz vein (borehole T–5, 60.8 m). Abbreviation: PPL: plane-polarized light.

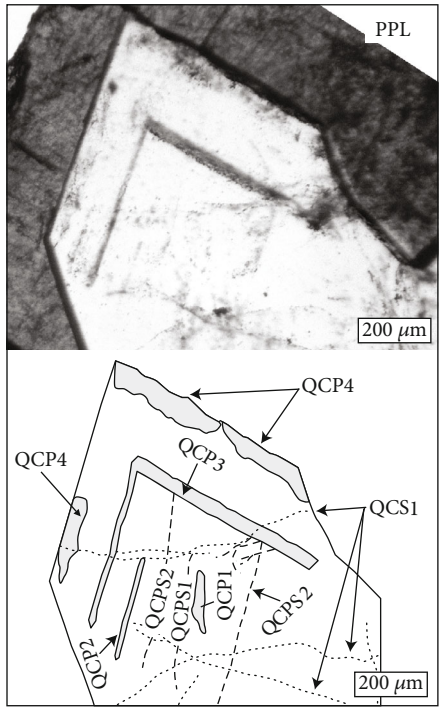

Figure 7: Photomicrograph and sketch about the arrangement of fluid inclusion assemblages (primary: QCP1 to QCP4, pseudosecondary: QCPS1 and QCPS2, secondary: QCS1) in a quartz single crystal from a quartz-carbonate vein (borehole Bm–1, 875.0 m). Abbreviation: PPL: plane-polarized light.

QP1, QP2, and QP3) can be distinguished, corresponding to the temporary sequence of the assemblages (Figure 6). Along healed microcracks, tiny (<2 μm) pseudosecondary and secondary assemblages rarely occur. They contain one-phase liquid, but they are inappropriate for exact microthermometry.

In the QP1 FIA, two-phase (liquid and vapor, L+V, respectively) inclusions are predominant. In the QP2 and QP3 assemblages, one-phase pure liquid (L) and two-phase (L+V) inclusions can be found in nearly equal amounts (Figure S5). Two-phase inclusions are liquid-dominant and their φ_{vap} values are in a range of 0.10–0.17 for QP1, while lesser then ~0.1 is typical for both QP2 and QP3. Shape of two-phase inclusions is generally irregular. Their size varies in a broad range from 5 to 30 μm, while one-phase inclusions usually are smaller in size (5–10 μm). Raman spectra acquired at room conditions (T_{lab}) from vapor and liquid phases of the inclusions indicate that their inclusion fluid is an aqueous-electrolyte solution without any volatile contents.

Regarding the QP1 to QP3 inclusions, ice nucleation occurred at low temperatures and T_n (ice) values varied between −75 and −62°C (Table S4). First melting phase during reheating of the inclusions occurred between −56 and −47°C. Last melting of ice occurred in the presence of salt hydrate crystals (hydrohalite, Hh: $NaCl * 2 \cdot H_2O$) based on the Raman spectra (Figure S5). T_m (ice) data scatter in a range from −27 to −21°C ($n = 37$; Tables 1 and S4). Hydrohalite crystals were melted after final ice melting in each case. The T_m (Hh) values vary in a broad range from −22 to −3°C ($n = 20$). During heating procedure, the homogenization of the studied inclusions occurred into liquid phase (L+V⟶L) without any exception. Homogenization temperatures (T_h) for QP1 FIA are in a broad interval from +88 to +145°C ($n = 18$); nevertheless, lower values are observable for QP2 and QP3 FIAs (T_h: from +63 to +89°C, $n = 10$ and T_h: from +50 to +77°C, $n = 14$, respectively; Tables 1 and S4).

4.4.2. Quartz-Carbonate Veins

(1) Quartz-Hosted Fluid Inclusions. Primary (P), pseudosecondary (PS), and secondary (S) FIAs occur in euhedral quartz crystals (Figure 7). Four primary FIAs are arranged along growth zones in the quartz phase (from QCP1 to QCP4, respectively). Besides primary ones, two pseudosecondary (QCPS1 and QCPS2) and one secondary (QCS1) FIAs can be observable. The relative temporary succession of these assemblages is the following: QCP1⟶QCPS1⟶QCP2⟶QCPS2⟶QCP3⟶QCP4-⟶QCS1. Two-phase liquid-vapor (L+V) and one-phase liquid (L) inclusions can be found in each primary FIA at room temperature (T_{lab}). In the QCP1, QCP2, and QCP3 assemblages, two-phase (L+V) and one-phase (L) inclusions can be found in nearly equal amounts but pure liquid (L) inclusions are in a higher proportion in the QCP4 assemblage. Most of the inclusions are irregularly shaped (Figure S6). Their longest dimension varies between 3 and

25 μm and the two-phase inclusions show a liquid-dominant character. In the primary FIAs, the φ_{vap} values are in the range of 0.02–0.12. Pseudosecondary and secondary FIAs consist almost solely of one-phase liquid (L) inclusions and their maximal dimensions are in a range of 2–10 μm. Based on Raman microscopy of vapor and liquid phases at T_{lab}, each FIA of quartz contains pure aqueous-electrolyte solution without any gaseous/volatile components.

During cryoscopic analyses, nucleation of a vapor bubble can be occurred in many one-phase (L) inclusions during cooling. This phenomenon was observable in each FIA refering to a vapor nucleation metastability that may occur frequently in these inclusions. Ice nucleation temperatures are between −86 and −51°C. The initial melting temperature of ice (T_i) occurred between −57 and −47°C in each FIA and most of the measured data are around −52°C. Additionally, Raman microscopy revealed the presence of hydrohalite crystals besides ice (Figure S6). The final melting temperatures of both ice and hydrohalite were measured during reheating procedure in each primary FIA. Last melting of ice occurred in the presence of hydrohalite crystal in each case. Similar melting temperatures are observable in each primary assemblage (QCP1 to QCP4). T_m (ice) values are between −28 and −21.7°C ($n = 39$) while T_m (Hh) values are in a broad range from −25 to −1.6°C (Tables 1 and S4). Two-phase fluid inclusions of the primary FIAs were homogenized into a liquid phase (L+V⟶L) in each case. The broadest range and the highest T_h values can be observed in the case of the QCP1 assemblage where the data vary between +54 and +153°C ($n = 18$). From QCP2 to QCP4, the T_h values can be found in a range of ~40–80°C ($n = 39$). Nevertheless, in the QCP3 and QCP4 FIAs, more and more values are lesser than +60°C (Tables 1 and S4).

(2) Carbonate-Hosted Fluid Inclusions. In the dolomite phase, fluid inclusions are not arranged along growing zones of the crystals, and inclusions along trails or healed microcracks are not observable. The inclusions made continuous clusters which fill the entire domain to the clear overgrowth band (Figure 8). This latter phase is almost free of fluid inclusions except few minor (<3 μm) ones which are inappropriate for microthermometry. The distribution of the studied inclusions follows the crystallographic directions, reflecting their primary origin hence fluid inclusions of dolomite can be classified into one primary originated FIA (DP1). Inclusions of DP1 mainly show two-phase (L+V) character (Figure S7) and one-phase (L) inclusions can be found in subordinate amounts. Regular, close to negative crystal-shaped inclusions are dominant but inclusions with an almost irregular shape can also be found among them. Their size is very variable, and their longest dimension is in a range of 5–20 μm. Two-phase inclusions are liquid-dominant and their φ_{vap} are in a range of 0.15–0.2.

Owing to the fluorescence of dolomite, it was extremely difficult to obtain suitable Raman spectra from the inclusions both at T_{lab} and lower temperature also. In a few cases where spectra were collected successfully, the shape of the curve

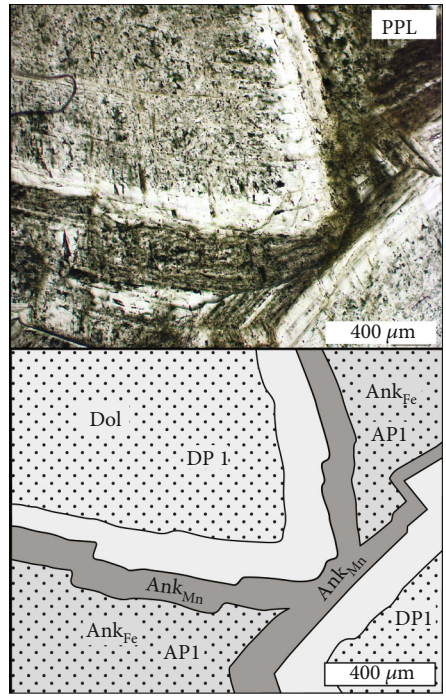

Figure 8: Photomicrograph and sketch about the arrangement of the primary fluid inclusion assemblages (DP1 and AP1) in Dol and Ank$_{Fe}$ phases from a quartz-carbonate vein (borehole Bm–1,875.0 m). Abbreviation: PPL: plane-polarized light; Dol: dolomite; Ank: ankerite.

indicates high-salinity aqueous-electrolyte character of the inclusion fluid without any dissolved volatile components (Figure S7). Ice nucleation temperatures are around −80°C and first melting occurs between −58 and −49°C. Last ice melting temperatures are in a range from −29 to −26°C ($n = 10$). Salt hydrate crystals were not able to detect visually in the inclusions; however, the T_i values propose the possible presence of this phase during reheating procedure. Since salt hydrate phases were detectable neither visually nor by using Raman signal, the last hydrate melting temperatures were not possible to detect in the FIA. The inclusions were homogenized into the liquid phase (L+V⟶L) during heating, and liquid to vapor homogenization was not observed. Homogenization temperatures are in a range of 127–167°C ($n = 14$; Tables 1 and S4).

In the Ank$_{Fe}$ phase, fluid inclusions are arranged along growing zones suggesting their primary origin (Figure 8). They are not separated by inclusion free growth bands; hence, they can be classified into one primary FIA designated by AP1. The AP1 assemblage contains irregular and negative crystal-shaped inclusions in nearly equal amounts and their size varies in a range of 5–17 μm similarly to the DP1 FIA. At room conditions (T_{lab}), two-phase (L+V) liquid-dominant (φ_{vap} = ~0.12) inclusions are predominant and one-phase (L) inclusions can be found in subordinate amounts. In spite of fluorescence of the host mineral, in some cases, suitable Raman spectra were collected at T_{lab}. The appearance of these spectra indicates low-salinity aqueous-

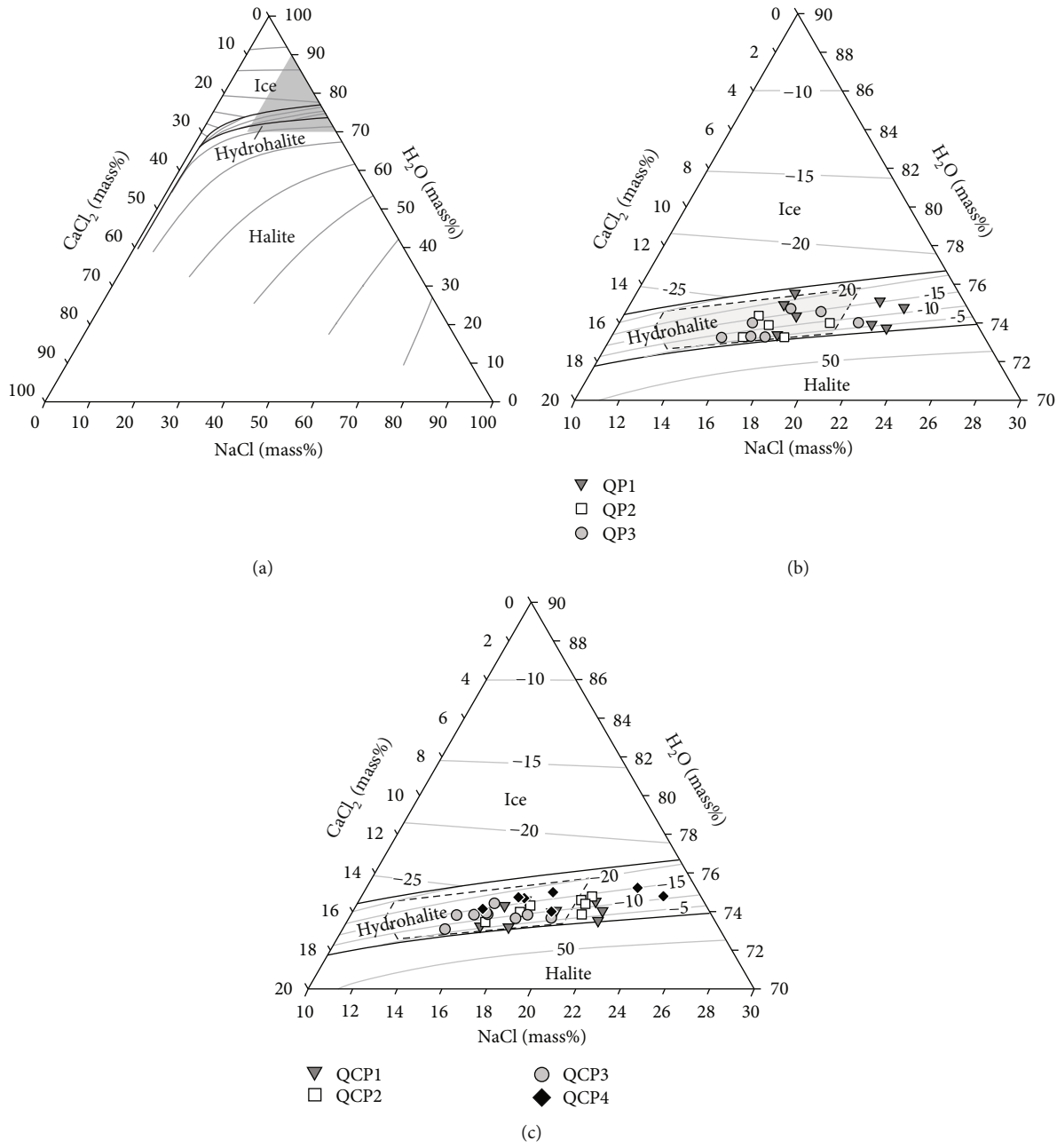

Figure 9: Salinity calculation of the inclusion fluids. (a) NaCl-$CaCl_2$-H_2O ternary phase diagram of the inclusion fluids; shaded triangle indicates the composition of the analyzed fluids. (b) Composition of the primary aqueous fluid inclusions in the quartz FIAs from quartz veins in the NaCl-$CaCl_2$-H_2O system. (c) Composition of the primary aqueous fluid inclusions in the quartz FIAs from quartz-carbonate veins in the NaCl-$CaCl_2$-H_2O system. For comparison, FI data from vein filling quartz of quartz-carbonate veins of a neighboring crystalline complex (Baksa Gneiss) [16] are also shown (shaded polygon; see discussion in the text).

electrolyte character of the fluid without any kind of volatile components (Figure S7).

During cooling procedure, ice nucleation occurred around −44°C in each case. First melting temperature was not possible to detect visually or by Raman spectroscopy. T_m (ice) values are in a very narrow range from −3 to −2°C in each inclusion ($n = 10$). Besides ice, other phases such as salt hydrate were not observable during reheating. Homogenization of inclusions occurred into a liquid phase (L+V⟶L) between 60 and 110°C ($n = 21$), and majority of the data are in a range from 80 to 100°C (Tables 1 and S4).

4.4.3. Composition of Inclusion Fluids. The abovementioned narrow range of initial melting temperatures of ice in the QP1 to QP3 and QCP1 to QCP4 FIAs indicates that the analyzed fluids can be modeled by the NaCl-$CaCl_2$-H_2O model system (Figure 9, Table 1). In the studied DP1 fluid inclusions, last melting temperatures of hydrohalites were not detectable; therefore, the composition of these inclusion

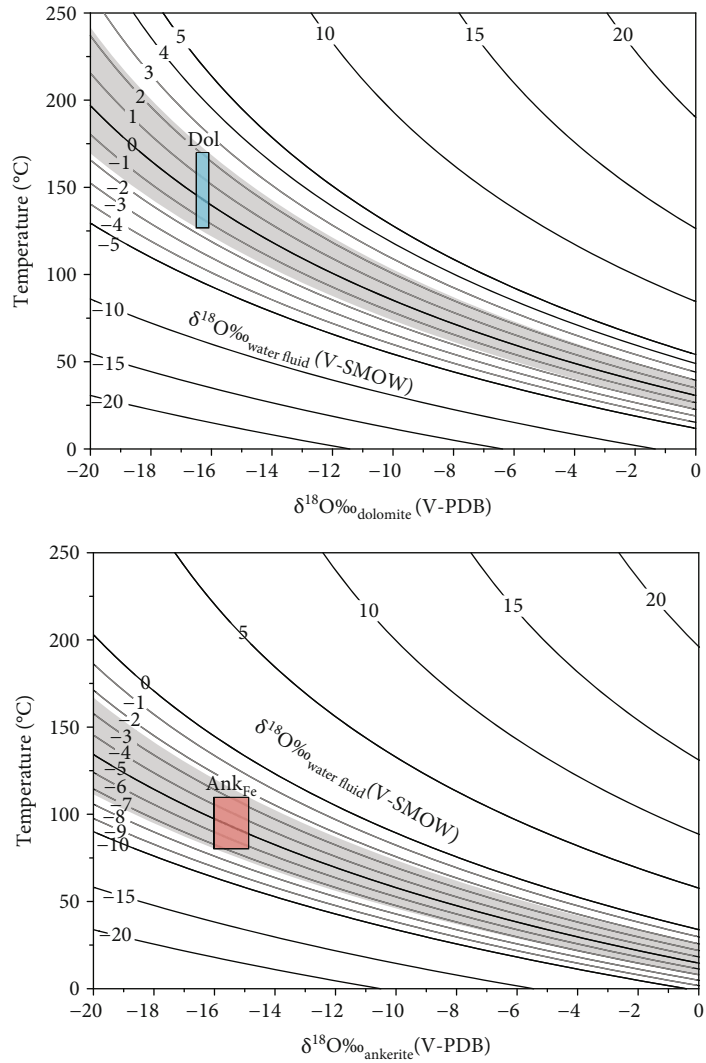

Figure 10: Calculated $\delta^{18}O$ values of the fluids entrapped in Dol and Ank_{Fe} using T_h data of the DP1 and AP1 FIAs, respectively. Fractionation equation of Hilgers and Urai [46] was used during calculations. (a) $\delta^{18}O_{dolomite}$ versus temperature for various $\delta^{18}O_{water}$ values. (b) $\delta^{18}O_{ankerite}$ versus temperature for various $\delta^{18}O_{water}$ values. The curved lines represent constant $\delta^{18}O$ values (V-SMOW) for water fluid.

fluids was calculated from last ice melting temperature data in the H_2O-$CaCl_2$ model system. Additionally, high T_m (ice) values indicate the presence of low-salinity inclusions in the AP1 FIA. Compositions of the related inclusion fluid were calculated in the H_2O-NaCl model system (Tables 1 and S4).

The $\delta^{18}O$ values of the mineralizing fluids can be determined using the $\delta^{18}O$ values of the dolomite and ankerite phases and the precipitation temperatures determined by fluid inclusion analyses above. Because the primary fluid inclusions of Dol (DP1) and Ank_{Fe} (AP1) do not show any evidences of post entrapment modifications, their T_h values can be interpreted as a minimum formation temperature range of the Dol and Ank_{Fe} phases. These temperature constraints were used together with the fractionation equation of Zheng [45] to calculate the oxygen isotope range of the Dol and Ank_{Fe} precipitating fluids, respectively. Nevertheless, since there was no opportunity for a pressure correction of T_h data, oxygen isotope values of the fluid are slightly underestimated (max. 1–2‰). The calculated $\delta^{18}O$ (V-SMOW) values of the parent fluid are in a range from −1.7 to +2.3‰ for DP1 FIA, while the calculated $\delta^{18}O$ (V-SMOW) values of the fluid are in a range from −7.3 to −2.3‰ for AP1 FIA (Figure 10).

5. Discussion

5.1. Paleoenvironmental and Paleofluid Features of the Studied Téseny Rocks

5.1.1. Vein Styles and Fluid Fingerprints. Vein-type mineralization in the Téseny rocks dominantly forms blocky morphological types with inclusion-rich quartz and carbonate crystals, suggesting their potential to contain information about origin and geological relationships of the mineralizing fluids. Two major kinds of fluids can be distinguished: (1)

quartz- and carbonate (dolomite)-hosted high-salinity aqueous fluids, and (2) carbonate (ankerite)-hosted low-salinity ones. The presented data suggest a paleohydrological communication between the crystalline basement and the overlying Téseny sedimentary rocks (see Figure 9) [17–19]. Therefore, the studied cross-formational fracture-vein systems can be interpreted as region-specific fluid mobilization events. As a novel approach, specific characteristics of the studied blocky veins (e.g., alteration and mineralization types, fluid compositions) in the study area are used for regional reconstructions (see discussion parts below).

Thin fibrous, stretched, and polytextured veinlets appear only in subordinate amounts in the study area; hence, their correlative merit is insignificant. Bedding-parallel veins of fibrous calcite and rare quartz, corresponding to the "beef" or "cone-structure" with sinusoidal inclusions [46, 47], reflect the diagenetic environment. The Pennsylvanian coal-bearing Téseny Sandstone is a mature/over mature source rock with a vitrinite reflectance of ~3.35% [23]; therefore, horizontal fractures could be a result of high pore fluid pressures during burial alteration of organic matter (hydrocarbon generation) [47].

5.1.2. Possible Correlation within the Tisia: Pennsylvanian Continental Records. In the Békés Unit (Figure 1), within the Hungarian part of the Tisia, several deep wells with intermittent coring near the town of Szeged (Great Hungarian Plain, Algyő Basement High) penetrated greenish gray rocks described as Carboniferous breccia [30]. This breccia unit contains randomly oriented angular mica schist, gneiss, and quartzite fragments (up to 10 cm in diameter) in a mica-rich matrix. Tentatively, these fossil-less rocks were regarded as continental deposits which are tectonically covered by a Triassic sedimentary succession [30, 48]. According to the detailed investigations, a network of dark fine-grained veins was also observed and these rocks were reconsidered as ultracataclasites. Therefore, the breccia was redefined as a tectonized part of the crystalline basement [48].

Both the fractured metamorphic basement rocks and the overlying Triassic sequences are hydrothermally altered, containing veinlets and dissolution vugs partially filled by saddle dolomite [49–51]. Under cathodoluminescence microscope, saddle dolomite crystals exhibit a marked zonation, whereas fluorescence microscopy reveals that significant part of the saddle dolomite crystals contains primary petroleum-bearing aqueous inclusion assemblages. Microthermometry performed on saddle dolomite-hosted FIAs suggests the presence of hot (135–235°C) and moderately saline brines (4–9 eq. mass% NaCl) during the precipitation [50]. This post-Middle Triassic vein generation differs from the dolomite-bearing veins in this paper. Therefore, there is no way to give an extensible correlation for Téseny rocks eastwards.

Southwards, in Croatia, the Slavonian Mountains (Figure 1) represent rare basement outcrops of the Tisia where three tectono-metamorphic complexes can be defined: Psunj, Papuk, and Radlovac Complexes [52–54]. The Radlovac Complex consists of very low- to low-grade metamorphic sequences largely composed of metapelites (slates and subordinate phyllites), metapsammites (metagraywackes), and metaconglomerates deposited in a shallow marine environment [54, 55]. In slates from the outcrop at Mt. Papuk, corresponding to the middle part of the metamorphic sequences, a Carboniferous (Westphalian) macroflora was reported [56]. It consists of *Asterophyllites*, *Pecopteris*, *Neuropteris*, and *Cordaites* plant assemblage. Therefore, representing similar developments, these metasedimentary rocks were tentatively correlated with the Téseny Sandstone Formation [30, 57].

The petrography and geochemistry of the Radlovac Complex, including provenance of the Pennsylvanian metapsammites, was extensively characterized in the last few years [54, 58, 59]. According to these authors, the most common metasedimentary rocks of the Radlovac Complex are fine-grained metapelites (more than 70% matrix) and moderately sorted metapsammites (less than 40% matrix). Both groups have similar mineral composition with dominant quartz, illite-muscovite, chlorite, and plagioclase, subordinate K-feldspar, paragonite, hematite, and rare carbonate minerals. Complex heavy mineral (monazite, xenotime) analyses suggested that one major source for the Radlovac Complex metasedimentary rocks was felsic igneous rocks of Variscan age. Additionally, the bulk chemistry for both metapelites and metapsammites pointed to felsic igneous rocks as protoliths, corresponding to the continental island arc geotectonic environment [54].

A dominant felsic protolith source is in good correlation with the provenance of the Téseny Sandstone, but this latter succession has a more immature framework composition with significant amounts of acidic volcanic and metamorphic rock fragments [21, 24]. In comparison whole-rock geochemical data of the Téseny Sandstone samples [21–24] with the published data from the Pennsylvanian metapsammites of the Slavonian Mts [54], a difference between their geochemical fingerprints is also obvious (Figure 11). The rock and mineral fragments in the Téseny sands and conglomerates were identifiable as coming from three sources: (1) a recycled Variscan orogenic area (collision suture and fold-thrust belt), indicated by the presence of metamorphic and sedimentary lithic fragments; (2) an uplifted plutonic (granite-gneiss) basement; and (3) an old (probably Variscan) magmatic arc, indicated by the lesser amounts of siliceous volcanic rocks [21, 24]. These findings strongly suggest that the depositional basin of the Téseny rocks was spatially and/or temporally isolated from the Radlovac sedimentary basin in South Tisia.

5.1.3. Paleofluid Fingerprint of the Hungarian Part of W Tisia (Mecsek–Villány Area). The distinct nature of the Pennsylvanian coal-bearing succession in the Slavonia–Drava Unit led to its paleohydrological comparison with the adjacent crystalline basement blocks (W Tisia; Figures 1 and 3). Within it, the Baksa Complex is the likely main source area for gneiss/metagranitoid and mica schist clasts from Téseny sediments. Additionally, crystalline plutonic rocks together with microgranite dikes in the Mórágy Complex (Kunság Unit, Mórágy Subunit) represent the principal fine-grained plutonic source (Téseny aplite clasts) that fed the Pennsylvanian sedimentary basin during deposition of the Téseny Sandstone Formation [24].

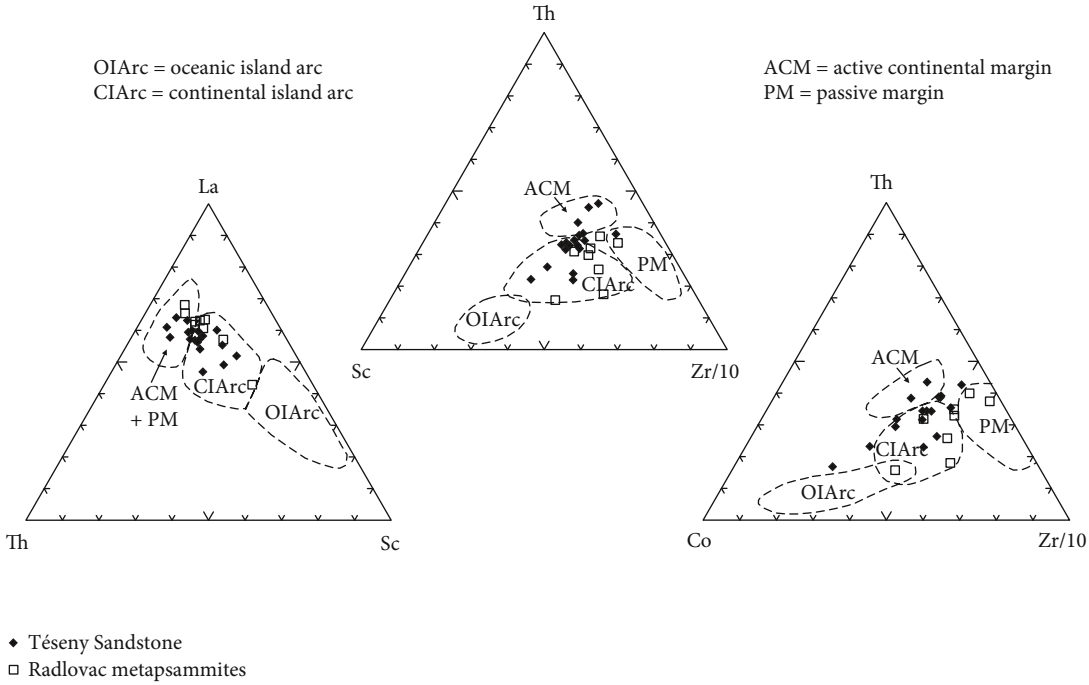

Figure 11: Ternary discrimination diagrams [60] display the compositional trends among the Téseny and Radlovac Pennsylvanian samples and confirm that these sediments were dominantly derived from different provenance areas. Data come from [24, 54], respectively.

In the polymetamorphic rock body of the Baksa Complex (Figure 3), a well-developed fracture filling network filled by Ca-Al-silicate minerals and/or sulfides (Fe-Zn-Pb; dominantly pyrite and sphalerite) was documented by previous authors [61–63]. In the silicate-rich paragenesis, clinopyroxene-dominant, epidote-dominant, and feldspar-dominant vein types were distinguished [17–19], following by quartz-carbonate (dolomite, calcite) veins in a later mineralization stage [16, 17].

A detailed investigation [17–19] revealed a characteristic diopside⟶epidote±clinozoisite⟶sphalerite⟶albite±K-feldspar⟶chlorite±adularia±prehnite⟶pyrite⟶calcite (calcite1+calcite2+calcite3) fracture filling mineral succession, reflecting propylitic affinity during the older hydrothermal events. Data from microthermometry of primary fluid inclusions in diopside (T_h: 276–362°C) and epidote (T_h: 180–360°C) together with their nearly identical salinities (0.7–2.9 and 0.2–1.2 eq. mass% NaCl, respectively) indicated that the corresponding mineralization occurred in a same high-temperature and low-salinity fluid environment [17, 19]. Unfortunately, there are not any fluid inclusion data from related feldspar phases.

The Ca-Al-silicate mineralization events also resulted in disseminated and vein-style sulfide mineralization in the Baksa Complex [17, 62, 63]. The veins which vary in thickness from 0.1 to 7 cm contain dominantly of common sulfides (pyrite, marcasite, pyrrhotite, sphalerite, chalcopyrite, galena, pentlandite, and covellite) and small amounts of quartz; additionally, rare hematite also occurs [62, 63]. Fluid inclusion studies of vein filling quartz crystals (T_h: 235–295°C and 3.5–5.1 eq. mass% NaCl) indicated a postmagmatic hydrothermal origin during cooling of a hydrothermal system [63].

Additionally, the crystalline host rocks (gneiss, mica schist) of the Baksa Complex are strongly altered, exhibiting extensive epidotization, chloritization, albitization, and sericitization [18, 61]. The pervasive hydrothermal leaching caused significant secondary porosity (cavities) in the altered domains which was partially filled by albite and epidote, and the total lack of the quartz phase is a characteristic feature of the metasomatized rocks. Fluid inclusions of cavity filling epidote show a similar character (T_h: 180–360°C; salinity: 0.2–1.6 eq. mass% NaCl) that can be found in the Ca-Al-silicate veins [18].

In the Baksa Complex, development of calcite was characterized by filling the remaining pore space in the Ca-Al-silicate veins (first and second populations of calcite) and formation of crosscutting veins (second and third populations of calcite). Microthermometry of primary inclusions of the subsequent calcite1 and calcite2 generations (T_h: 75–124°C, 17.5–22.6 eq. mass% $CaCl_2$ and T_h: 106–197°C, 2.9–6.3 eq. mass% NaCl, respectively) reflects a significant change in the evolution of the vein system [19]. Based on the high salinity and low T_h range of the earliest calcite, this carbonate phase was precipitated from downward-penetrating sedimentary brines or from descending meteoric water that infiltrated through evaporite bodies [17, 19]. This interpretation was also supported by low values of the calculated fluid $\delta^{18}O$ (−13 to −4‰, V-SMOW). Calcite in the Ca-Al-silicate veins, therefore, can represent the subsequent fluid circulation that led to precipitation of quartz, dolomite, and calcite in the quartz-carbonate veins [19].

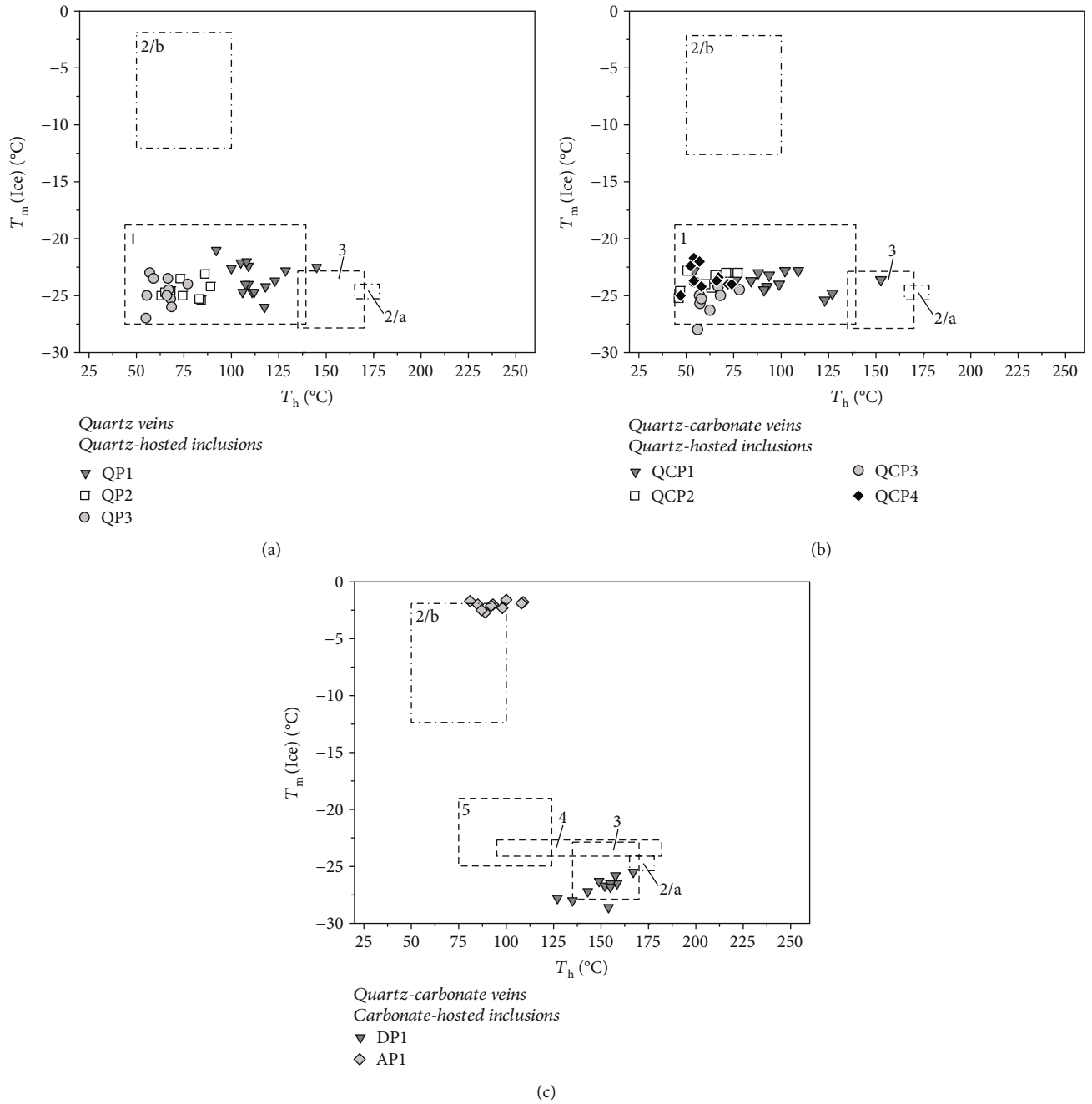

Figure 12: Paleofluid fingerprint of the studied FIAs. (a) T_h vs. T_m (ice) plot of the primary inclusions of quartz from quartz veins. (b) T_h vs. T_m (ice) plot of the primary inclusions of quartz phase from quartz-carbonate veins. (c) T_h vs. T_m (ice) plot of the primary inclusions of dolomite and Ank_{Fe} phases of quartz-carbonate veins. For comparison, the numbered boxes correspond to the fluid inclusion data from different geological localities exhibiting characteristic post-Variscan vein mineralizations (see discussion in the text). 1—FI data from vein filling quartz of quartz-carbonate veins of Baksa Gneiss Complex [16]; 2—FI data from Bohemian Massif [66]; 2/a represents FI data from early quartz while 2/b represents FI data from late-stage quartz of post-uranium stage mineralization of Rožná uranium deposits; 3—FI data from post-Variscan veins of Oberpfalz [67, 68]; 4—FI data from dolomite of quartz-carbonate veins of Baksa Gneiss Complex [16]; 5—FI data from calcite1 phase of Ca-Al silicate-dominant veins of the Baksa Gneiss Complex [19].

In the postmetamorphic quartz-carbonate veins, corresponding to a relatively late mineralization stage mentioned above, a quartz⟶dolomite+calcite (cc1)⟶calcite (cc2) mineral sequence was observed, and traces of high-salinity fluids were detected [16, 17]. The T_h values of the quartz-hosted primary FIAs are between 44 and 139°C. The dissolved salt content is very high in each fluid inclusion, exhibiting a NaCl-dominant composition (20.1–25.6 eq. mass% NaCl) with a minor amount of $CaCl_2$ (1.5–6.0 eq. mass%). Additionally, in the vapor phases of each FIA, CH_4 and N_2

contents were detected by Raman microspectroscopy [16]. Regarding carbonate-hosted (dolomite and cc1) inclusions, the T_h values can be found in a range of 95–182°C, whereas estimated salinity data are between 23.9 and 24.6 eq. mass% NaCl. These salt-rich paleofluids probably were originated from the Permian and/or Triassic evaporites of the region, reflecting a significant fluid migration event between the crystalline basement and the overlying sediments [16, 17].

In the westernmost part of the studied area (Figure 3), near the village of Dinnyeberki (Mórágy Complex, borehole 9017), fine quartz and uranium ore-bearing carbonate veinlets were documented in the weakly to moderately altered Mórágy-type granitoids [64, 65]. Economically insignificant uranium ore veinlets were developed along the fractures of the mylonitized granitoid rocks [65]. The earliest veins are thin quartz veinlets containing quartz and rare chlorite, whereas during a later substage, fractures were filled up by carbonates which gave rise to several populations of calcite (and minor dolomite and siderite) veins. Mineralization in carbonate veins forms uraninite, coffinite, pyrite, and calcite; additionally, U-Ti-oxides (such as brannerite), monazite, Th-silicate minerals, rare xenotime, and zircon also occur. Aggregates of spherulitic or irregularly shaped accumulations of uraninite are usually rimmed by coffinite. This latter mineral commonly forms rims around pyrite grains. The uranium minerals show complex chemistry with elevated P, Y, and rare-earth elements (REEs). This vein-type uranium mineralization might represent ascendant hydrothermal (epi-telethermal) mineralizing fluids genetically related to an Alpine rejuvenation of an earlier pre-Alpine event [65].

It is important to note that pilot studies [17–19] suggested that there could be a paleohydrological communication between the crystalline basement and the overlying Téseny sedimentary rocks during the cementation phase resulted in quartz-carbonate veins. Based on the results above, quartz- and dolomite-hosted high-salinity aqueous fluids can represent the same mineralization stage in both Téseny and Baksa rocks (Figures 9 and 12). Furthermore, a probable genetic relationship was proposed between the Ca-Al silicate vein networks of the neighboring Baksa Complex (i.e., alkali feldspar-dominant vein type with an albite±K-feldspar⟶chlorite±adularia±prehnite⟶pyrite⟶calcite mineral assemblage) and similar veins (quartz-silicate-carbonate blocky veins) in the Téseny rocks [25].

5.2. Paleofluid Evolution of the W Tisia and Its Relation to the Variscan Europe. As discussed above, the evolution of hydrothermal mineralization and host rock alteration in the Hungarian part of the W Tisia (Mecsek–Villány area) comprises several major stages. In this section, we provide a comprehensive set of fluid inclusion analyses from the studied area together with published data come from the Variscan Europe, especially from the Moldanubian Zone of the Bohemian Massif to test the presumed paleogeographic relationship between them.

In the Hungarian part of the W Tisia, the first stage is characterized by chloritization, epidotization, and sericitization of the metamorphic rocks together with subsequent formations of Ca-Al-silicate and quartz-sulfide veins in the Baksa Complex (diopside⟶epidote±clinozoisite⟶sphalerite (pyrite) fracture filling mineral succession) [17–19, 62, 63]. The corresponding fluid inclusion record consists of high-temperature and low-salinity aqueous inclusions. It was previously proposed [18] that this paragenesis could indicate a wall rock alteration related to the propylite metasomatic family; however, widespread chloritization, sericitization, and pyritization, at least partially, can also connect with a generally reduced retrograde-metamorphic fluid phase [66]. Regarding timing of related hydrothermal events, $^{40}Ar/^{39}Ar$ and K–Ar ages for white mica from amphibolite facies rocks within the metamorphic basement of the W Tisia range from 307 to 312 Ma [69]. Formation of white mica in the study area coincides with the postorogenic extension of the Variscan crust and with the accompanying rapid exhumation of the orogenic root [70], resulted in the retrograde-metamorphic equilibration of the high-grade metamorphic host rocks during the Late Westphalian (e.g., Massif Central and Bohemian Massif [66, 71], respectively). It can be, therefore, suggested that the origin of fluids giving rise to the clinopyroxene-dominant and epidote-dominant mineralization at Baksa was related to a greenschist-facies retrograde reequilibration of their amphibolite facies mineral paragenesis (Figure 13). This interpretation fits in with the total lack of the clinopyroxene- and epidote-dominant vein types in the Westphalian Téseny rocks.

On the other hand, corresponding to the fracture filling network filled by Ca-Al-silicate minerals at Baksa, hematite-rich alkali feldspar-dominant vein type with chlorite (± epidote) and calcite also appears in the studied Téseny Sandstone (Figure S2). Additionally, mineralogical and petrographic features of albitization, chloritization (authigenic Mg-chlorite), and carbonatization were documented in the host sandstone (Figure 4 and [23, 24]). Obviously, this mineralization stage can be related to a generally oxidized alkaline fluid phase and could be significantly separated in time from the previous one. The presence of hematite in the first-stage quartz-sulfide veins [62, 63], conspicuously as a later phase mineral, reflects the cross-formational character of the parent fluid, whereas the high salinity and low T_h range of the FIA for the latest stage calcite in the Baksa Ca-Al-silicate veins could support the proposed effect of descending fluids [16, 17].

In the Mecsek Mountains (Figure 3), the Permian sedimentary record contains playa lake and saline mudflat deposits (Boda Claystone Formation; Kungurian to Capitanian), including evaporites such as gypsum, anhydrite, and rare pseudomorphs after hopper halite [72–75]. Consequently, Na-rich playa fluids were available during the Late Permian in the study area. Crosscutting monomineralic quartz and quartz-carbonate veins with high-salinity aqueous inclusions both in the Baksa and Téseny rocks are, more probable, in connection with the playa brines. Additionally, high-salinity fluids (T_h: 75–123°C, T_{fm} (ice): −24.6 to −16.9°C) were also identified in a metamorphic quartz lens from the Mecsekalja Zone metamorphic complex (Figure 3). They are possibly related to an active period of either of the fault generations crosscutting the Mórágy

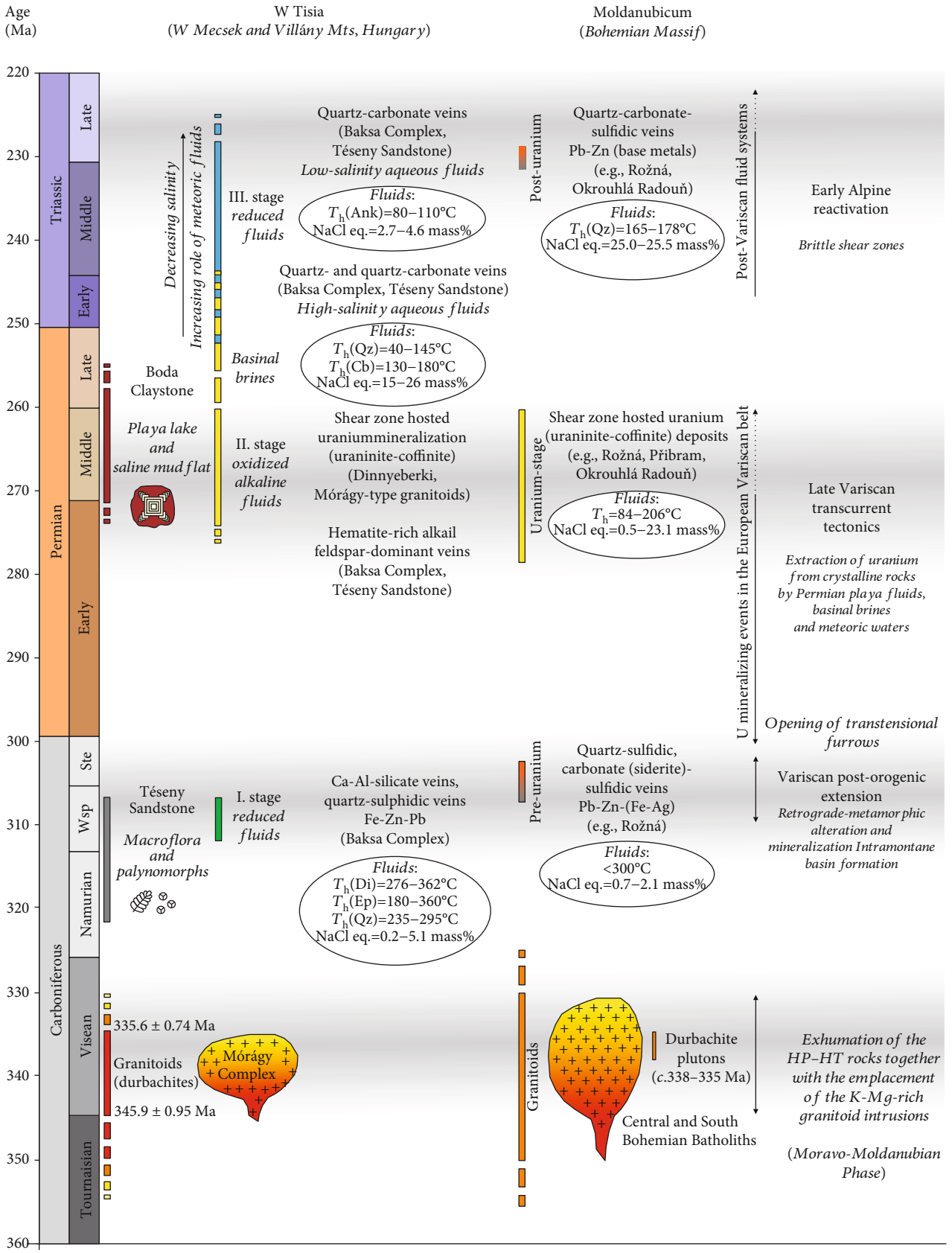

Figure 13: Evolution of hydrothermal mineralization of the W Tisia (Mecsek–Villány area) together with the most important mineralizing events in the Central European Variscan belt (Moldanubicum) [2, 3, 66, 83–86]. Abbreviations: Wsp: Westphalian; Ste: Stephanian.

Complex. The high-salinity fluid generation can be related to a regional fluid flow event predated the Mesozoic brittle deformation of the Mecsekalja Zone and is considered as being derived from evaporitic sequences of the above-lying sedimentary pile [76, 77]. This observation supports the timing of the high-salinity fluid flow event during the Late Permian. However, the appearance of galena and ankerite in the subsequent mineral paragenesis clearly indicates that their parent fluids derived from a more reductive environment, representing another mineralization stage during the post-Permian (Triassic?).

Unfortunately, there are not any clear evidences for timing of this second (Late Variscan) and third (post-Variscan or Early Alpine) mineralization stages. However, in the Téseny quartz-silicate-carbonate blocky veins, chlorite is locally accompanied by euhedral monazite and/or xenotime together with pyrite and other opaque minerals (Figure S3). Furthermore, the alteration of the Téseny wall rock is characterized by dissolution of quartz from the framework grains followed by albitization, carbonatization, and chloritization (Figure 4). This strongly suggests that the second event may overlap with the Mórágy-type granite-hosted, vein- or fault-type uranium mineralization at Dinnyeberki [65], forming a peripheral part of the alteration halo in the lower part of the Téseny succession. As a consequence, the related alkaline fluids are considered to be of crucial importance for correlation with the Late Variscan large-scale hydrothermal events.

Hydrothermal mobilization of REEs and Y is strongly related to the mobilization of Zr and U and generally indicates an influx of oxidized alkaline fluids [78, 79]. The relative synchronous age of the U mineralizing events in the European Variscan belt (300–270 Ma) could suggest a similar mineralization condition, with long-term upper to middle crustal infiltration of oxidized fluids likely to have mobilized U from fertile crystalline rocks during the Pennsylvanian to Permian crustal extension events [80]. Alteration resulted in intensive leaching of quartz, pervasive albitization, and subsequent chloritization is characteristic for the formation of episyenites (aceites) described from numerous uranium deposits of the European Variscan belt [80–86], including hydrothermal vein-type, fault- and shear zone-hosted uranium deposits [66]. Within it, the Bohemian Massif is the most important uranium ore district in Europe [66, 83–85] where episyenitization and the associated uranium mineralization occur not only in granites (e.g., Schlema-Alberoda, Annaberg, Příbram, Okrouhlá Radouň, Lower Silesia) but also in high-grade metamorphic rocks (e.g., Vítkov II, Okrouhlá Radouň, Rožná, Olší).

In the Moldanubian Zone of the Bohemian Massif, based on the previous papers [66, 84, 86], the origin of the uranium mineralization is associated with an infiltration of oxidized, alkaline Na-rich playa fluids and/or basinal brines of the Upper Stephanian and Lower Permian basins into the crystalline basement along deep brittle structures that opened during the Late Variscan transcurrent tectonics and furrows formation (Figure 13). Infiltration of brines effectively leached uranium from U-bearing minerals in the crystalline rocks. During the subsequent mineralization event (280–260 Ma, "uranium" stage or "ore" stage [66, 86], respectively), newly formed albite is typically stained by hematite. Additionally, a very small amount of adularia (K-feldspar) was locally crystallized. In the chloritized and pyritized zones of cataclasites, uranium together with several Ti, Zr, Y, P, and REEs phases was gradually precipitated due to the interaction of ore fluids with reducing host rock components. Post-uranium mineralization, corresponding to the Early Alpine transtension (240–220 Ma), resulted in quartz-carbonate-sulfide veins [66, 83].

Fluids from pre-uranium quartz-sulfide and carbonate-sulfide mineralization at the Rožná deposit have low salinities (0.7–2.1 eq. mass% NaCl), and primary inclusions were trapped at temperatures close to or lower than 300°C [66]. Calculated oxygen isotopic composition of fluids (fluid δ^{18}O, SMOW) was in a range from +7 to +8‰ for siderite-sulfidic mineralization, whereas it was about +3‰ for pre-uranium albitization [83]. For uranium stage, T_h of the primary aqueous inclusions in quartz and carbonates range from 84°C to 206°C. The salinities are highly variable and range from 0.5 to 23.1 eq. mass% NaCl resulted in the large-scale mixing of basinal brines with meteoric water [66, 83]. Regarding fluids from post-uranium mineralization, early quartz contains high-salinity (25.0–25.5 eq. mass% NaCl) primary aqueous inclusions with T_h of 165–178°C, whereas lower salinity and T_h values in paragenetically younger minerals indicate low temperatures (<100°C) of the latest stage of fluid activity [66]. Calculated fluid δ^{18}O value (SMOW) was close to 0‰ [83].

A similar evolution of fluid types is characteristic at the Okrouhlá Radouň deposit (Figure 13). Albitization was caused by circulation of alkaline, oxidized, and Na-rich playa fluids, whereas basinal/shield brines and meteoric water were more important during the post-ore stage of alteration, corresponding to the post-uranium stage [66]. In this area, fluid δ^{18}O values (V-SMOW) of post-ore calcite vary between −8.0 and +2.4‰ [87].

Very similar Late Variscan and post-Variscan hydrothermal events were published from the neighboring area of the Bohemian Massif (Harz, Black Forest, Oberpfalz; Figure 1) [67, 68]. These authors suggested that characteristic fluid systems with distinctive differences (e.g., fluids associated with metamorphism, Permian basinal brines) are regionally distributed in the Central European Variscan belt.

5.3. Paleogeographic Position of the W Tisia (Hungary). The previous published correlations have revealed several similarities in Variscan (Mississippian) evolution of the studied area (W Tisia) and the Moldanubian Zone of the Bohemian Massif [2, 3, 87]. For this reason, as a first step, we turned our attention to the Visean plutonic rocks (Figure 13). Significant and widespread durbachites seem to represent a distinct magnesio-potassic magmatic rock type derived from a strongly enriched lithospheric mantle source that is particularly characteristic for the European Variscan basement areas [88]. Within the Moldanubian sector of the Bohemian Massif, the emplacement of the (ultra-)potassic intrusions took

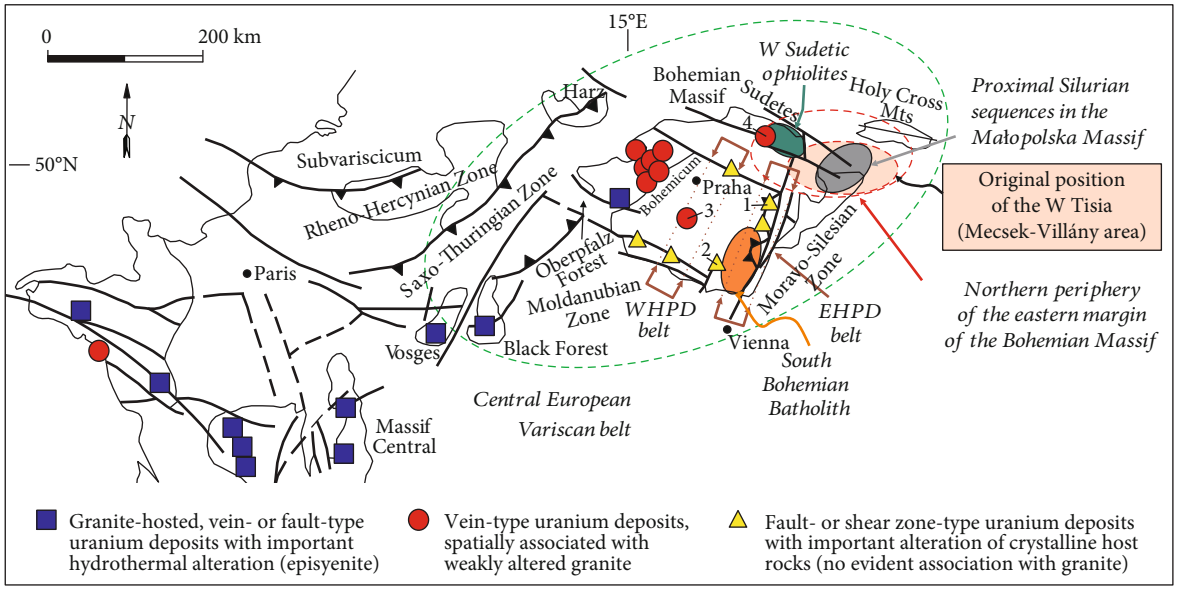

Figure 14: Paleogeographic relationships of the W Tisia in the framework of the European Variscan basement areas [1, 8, 66–68, 89, 95]. 1—Rožná deposit; 2—Okrouhlá Radouň deposit; 3—Příbram deposit; 4—Lower Silesia. Abbreviations: WHPD: western HP and Durbachite belt; EHPD: eastern HP and Durbachite belt.

place immediately after the tectonic ascent of the high-pressure (HP) rocks during a relatively narrow time interval between 335 and 338 Ma [89, 90]. It has been suggested that these durbachite plutons can be subdivided into two parallel belts, corresponding to the western HP and Durbachite belt and the eastern one [89].

Apart from the widespread Barrovian-style regional metamorphism, the combined occurrence of a granitoid (durbachite) pluton and HP rocks was also reported in the W Tisia [2–4, 87, 91, 92]. High-K and high-Mg granitoids found near Mórágy, 50 km northeast of the study area, show great similarities to the intrusions in the eastern part of the South Bohemian Batholith (Rastenberg) [2]. Using U-Pb geochronology on zircon crystals from the Mórágy Complex, the genetic picture of the Mórágy granitoid pluton was refined [93], showing a bimodal age distribution (335.6 ± 0.74 Ma and 345.9 ± 0.95 Ma) and suggesting a continuous crystallization in a long-time interval (Figure 13).

On the other hand, HP metamorphism was proven by analyses of the eclogite and amphibolite in the Baksa Complex [87, 91, 92, 94]. In the SW Tisia, the eclogite shows great similarities to the eclogites of the Monotonous Series of the Moldanubian Zone. Additionally, K-Ar geochronological data on amphibole from garnetiferous amphibolite show 348 ± 13 Ma cooling ages [87]. Furthermore, mafic and ultramafic rocks of the Baksa Complex likely represent different segments of a juxtaposed consuming ocean. A subduction-related metamorphic evolution led to HP metamorphism of the lower amphibolite unit of the Baksa Complex which was exhumed during a later phase, probably due to reversal of the transport direction from subduction to uplift [92]. The relict evidences for a Variscan tectono-metamorphic event, possibly corresponding to the Moravo–Moldanubian Phase (345–330 Ma [89]), strongly suggest a genetic relationship between the crystalline rocks of the W Tisia and the eastern HP and Durbachite belt of the Bohemian Massif.

Spatially associated with the Variscan medium-grade metamorphic rocks of the Baksa Complex and with the Mórágy granitoids, serpentinites also occur (Gyód and Helesfa serpentinite bodies, respectively) in the W Tisia (Figure 3). According to a recent publication [95], there exists a broad similarity in the composition and evolution between these serpentinites and similar rocks of some Sudetic ophiolites (Góry Sowie Massif in the West Sudetes). The aforementioned data seem to fix the original position of the W Tisia basement within the northern periphery of the eastern margin of the Bohemian Massif (Figure 14).

As mentioned above, another important feature of the study area is the presence of uneconomical uranium ore-bearing veinlets in the weakly to moderately altered Mórágy-type granitoids (Dinnyeberki) [65]. Regarding the hydrothermal uranium deposits of the Bohemian Massif [66], a vein-type deposit associated with weakly altered granite was documented in its northern part (Lower Silesia) which could indirectly support the W Tisia paleogeographic position suggested above (Figure 14). Other scenarios suggesting a connection of the Tisia to the southeastern [5] or southern/southwestern [14] part of the Bohemian Massif can be excluded because their hydrothermal uranium deposits reflect no evident association with granite plutons [66]. Therefore, a strong relationship between the study area and the Moldanubian part of the Bohemian Massif is also impossible. In accordance with the proximal character of the Silurian in the study area [1], the original position of the composite segments of the W Tisia (Mecsek–Villány area, Figure 2) is presumably to the northeast from the Bohemian Massif at the Late Paleozoic, north to the Moravo-Silesian Zone.

6. Conclusions

Based on detailed petrographic and geochemical investigations as well as fluid inclusion analyses, the following conclusions can be drawn about the studied basement rocks:

(1) Four vein types can be distinguished in the Téseny Sandstone Formation (W Tisia, Hungary), corresponding to the blocky, fibrous, stretched, and polytextured veins. According to the composition of the blocky veins, two major kinds of mineralizing fluids can be distinguished: (1) quartz- and carbonate (dolomite)-hosted high-salinity aqueous fluids and (2) carbonate (ankerite)-hosted low-salinity ones. Our data show an obvious paleohydrological communication between the crystalline basement (Baksa Complex) and the overlying Téseny sedimentary rocks

(2) In the western part of the Tisia (Mecsek–Villány area, S Hungary), the evolution of hydrothermal mineralization and host rock alteration comprises three major stages. The first event can only be detected in the metamorphic rocks (clinopyroxene-dominant and epidote-dominant mineralization at Baksa), corresponding to a reduced retrograde-metamorphic fluid phase during the Late Westphalian (~310 Ma). The second event can be related to a generally oxidized alkaline fluid phase with a cross-formational character (hematite-rich alkali feldspar-dominant veins). The quartz- and dolomite-hosted high-salinity aqueous fluid inclusions probably were originated from the Upper Permian Na-rich playa fluids of the region. The parent fluid of the third mineralization stage (ankerite-hosted inclusions) was derived from a more reductive and low-salinity environment and can represent a post-Variscan fluid system with an increasing role of meteoric fluids

(3) Based on the observed paleofluid fingerprints, the study area belonged to the Central European Variscan belt up to the Early Alpine orogenic phases. Its original position is presumably to the northeast from the Bohemian Massif, north to the Moravo-Silesian Zone, at the Late Paleozoic

A fundamental conclusion that can be drawn from our data derived from the Hungarian part of the W Tisia is that the major vein mineralization stages and host rock alteration styles reflect the effects of the characteristic hydrothermal events of the Central European Variscan belt. Therefore, as an independent tool, paleofluid fingerprints can be used to interpret the paleogeographic position of the studied area.

Data Availability

The petrographic, geochemical, and fluid inclusion data used to support the findings of this study are included within the article.

Conflicts of Interest

The authors declare that there is no conflict of interest regarding the publication of this paper.

Acknowledgments

For petrographic analysis of the Pennsylvanian Téseny rocks, Mining and Geological Survey of Hungary (Dept. of Geological and Geophysical Collections, Budapest) provided thin section collection from borehole Bm–1. We thank György Szakmány and Sándor Józsa (Eötvös Loránd University, Budapest), Zoltán Máthé (Mecsekérc Ltd., Pécs), and Bálint Péterdi (Mining and Geological Survey of Hungary) for the studied samples. The authors are grateful to Tivadar M. Tóth (University of Szeged) and Ronald J. Bakker and Federica Zaccarrini (Montanuniversität Leoben) for their supports during analytical measurements. This work was financially supported by the University of Szeged Open Access Fund (4389), the Bolyai Research Scholarship of the Hungarian Academy of Sciences (BO/266/18), the National Research, Development and Innovation Fund (OTKA K 108375), the New National Excellence Program of the Ministry of Human Capacities (ÚNKP-18-4-SZTE-16), and the New National Excellence Program of the Ministry for Innovation and Technology (ÚNKP-19-4-SZTE-34).

Supplementary Materials

Figure S1: typical blocky vein types of Téseny Sandstone. (a) Blocky quartz vein with euhedral quartz (Qz) crystals and goethite together with morphological sketch of this vein type (borehole T–5, 60.8 m). (b)–(d) Elongate blocky quartz veins together with morphological sketch of this vein type (samples T–7/1, 148.8 m and T–7/3, 150.6 m, respectively). (e) and (f) Characteristic fine-scale growth zonation patterns of quartz crystals of blocky textured quartz vein indicated in CL image. (g) and (h) Anhedral adularia (Adl) grains with turbide internal habit in the elongate blocky quartz vein type (sample T–7/3, 150.6 m). Detrital K-feldspar grains with a bright blue CL in the host sandstone are partially or totally replaced by brown-luminescent adularia in the vein. (i) Blocky textured carbonate (dolomite) vein and its morphological sketch (borehole Bm–1, 973.8 m). Other abbreviations: PPL: plane-polarized light; XPL: crossed polars; CL: cathodoluminescence image. Figure S2: characteristic polymineralic blocky vein types of Téseny Sandstone. (a)–(c) Quartz-carbonate vein type and its morphological sketch (borehole Bm–1, 875.0 m). (d) and (e) Euhedral quartz crystal deposited on the vein wall exhibiting fine-scale growth zoning indicated by fluid inclusion assemblages (borehole Bm–1, 875.0 m). (f) Petrographic characteristics of different carbonate phases can be found among the euhedral quartz crystals in the quartz-carbonate vein type. Note the curved crystal faces of the dolomite. (g) Dolomite crystals with sweeping extinction (borehole Bm–1, 875.0 m). (h) Subhedral galena crystal with typical triangular pits (borehole Bm–1, 875.0 m). (i) In the quartz-carbonate vein type, a distinct pattern of luminescence zoning representing different

carbonate generations is observed. Note the calcite solid inclusions with bright orange CL within the ankerite zones. (j)–(l) Characteristic appearances of quartz-silicate-carbonate veins together with the morphological sketch of this vein type (sample T–3/1, 95.3 m and borehole Bm–1, 1290.5 m, respectively). Abbreviations: Qz: quartz; Cb: carbonate; Dol: dolomite; Ank: ankerite; Gn: galena; Chl: chlorite; Fsp: feldspar; Ep: epidote; Py: pyrite; PPL: plane-polarized light; XPL: crossed polars; CL: cathodoluminescence image; RL: reflected light. Figure S3: characteristic polymineralic blocky vein types of Téseny Sandstone. (a)–(d) In the lowermost part of the Pennsylvanian section (borehole Bm–1 1062.1 m, covered thin section), organic material, chlorite, and/or pyrite are accompanied by euhedral monazite and/or xenotime crystals. Note: crosscutting relationships are also visible (hematite-rich alkali feldspar-dominant vein⟶veins with chlorite+monazite/xenotime⟶carbonate vein). Abbreviations: Cb: carbonate (calcite); Chl: chlorite; PPL: plane-polarized light; XPL: crossed polars. Figure S4: fibrous, stretched, and polytextured vein types of Téseny Sandstone. (a)–(c) Fibrous carbonate and quartz-carbonate veins with antiaxial growth morphology (borehole Bm–1, 927.0–929.4 m). (d)–(f) Fibrous carbonate vein with typical sinusoidal host rock fragments (borehole Bm–1, 901.5–904.2 m). (g) Stretched quartz vein with small amount of chlorite on the vein wall (borehole Bm–1, 1224.7 m). (h) and (i) Polytextured carbonate vein with fibrous texture on the vein wall and blocky one in the middle part of the vein (borehole Bm–1, 1027.6 m). Abbreviations: Cb: carbonate; Qz: quartz; Chl: chlorite; XPL: crossed polars. Figure S5: fluid inclusion petrography and microthermometry. (a) Two-phase liquid-dominant fluid inclusions in the QP1 FIA. (b) Hydrohalite crystal in a primary inclusion from the QP1 assemblage. (c) Raman spectrum of the hydrohalite and ice assemblage (borehole T–5, 60.8 m). Figure S6: fluid inclusion petrography and microthermometry. (a) Liquid-dominant primary fluid inclusion from the QCP3 FIA of quartz. (b) Phase equilibria among liquid, vapor, ice, and hydrohalite in a FI of the QCP1 FIA. (c) Metastable phase equilibria in a QCP2 inclusion. (d) Representative Raman spectrum of hydrohalite and ice from a primary FI of quartz from a quartz-carbonate vein (borehole Bm–1, 875.0 m). Figure S7: fluid inclusion petrography and microthermometry. (a) Representative primary inclusion (DP1) of the dolomite phase. (b) Fluid inclusion in the AP1 assemblage, showing tapered tips in the grow direction of the crystals. (c) Characteristic Raman spectra of fluid inclusions at T_{lab} from the DP1 and AP1 fluid inclusion assemblages (borehole Bm–1, 875.0 m). Table S1: chemical composition of the studied carbonate phases of the selected quartz-carbonate veins. Table S2: semiquantitative chemical composition of the studied galena samples. Table S3: stable isotope composition (in per mil) of the studied carbonate phases of the selected quartz-carbonate veins. Table S4: petrographic characteristics and microthermometric data of the studied fluid inclusions (individual measurement data). Abbreviations: T_n: nucleation temperature of ice; T_i: initial melting temperature of ice; T_m (ice): temperature of final melting of ice; T_m (Hh): temperature of final melting of hydrohalite; T_h: temperature of homogenization; p_h: pressure of homogenization; QP: primary fluid inclusions trapped in quartz from quartz veins; QCP: primary fluid inclusions trapped in quartz from quartz-carbonate veins; DP: primary inclusions trapped in dolomite; AP: primary inclusions trapped in ankerite. Note: notation refers to the temporary sequence of the assemblages (from 1 to 4, respectively). *(Supplementary Materials)*

References

[1] E. Mészáros, A. Varga, B. Raucsik, Z. Benkó, A. Heincz, and C. A. Hauzenberger, "Provenance and Variscan low-grade regional metamorphism recorded in slates from the basement of the (SW Hungary)," *International Journal of Earth Sciences*, vol. 108, no. 5, pp. 1571–1593, 2019.

[2] G. Buda, F. Koller, and J. Ulrych, "Petrochemistry of Variscan granitoids of Central Europe: correlation of Variscan granitoids of the Tisia and Pelsonia terranes with granitoids of the Moldanubicum, Western Carpathian and Southern Alps. A review: part I," *Acta Geologica Hungarica*, vol. 47, no. 2-3, pp. 117–138, 2004.

[3] U. S. Klötzli, G. Buda, and T. Skiöld, "Zircon typology, geochronology and whole rock Sr–Nd isotope systematics of the Mecsek Mountain granitoids in the Tisia Terrane (Hungary)," *Mineralogy and Petrology*, vol. 81, no. 1–2, pp. 113–134, 2004.

[4] T. Szederkényi, J. Haas, A. Nagymarosy, and G. Hámor, "Geology and history of evolution of Tisza Mega-Unit," in *Geology of Hungary*, J. Haas, Ed., Springer Verlag, Berlin, 2012.

[5] J. Haas, G. Hámor, and L. Korpás, "Geological setting and tectonic evolution of Hungary," *Geologica Hungarica Series Geologica*, vol. 24, pp. 179–196, 1999.

[6] L. Csontos and A. Vörös, "Mesozoic plate tectonic reconstruction of the Carpathian region," *Palaeogeography, Palaeoclimatology, Palaeoecology*, vol. 210, no. 1, pp. 1–56, 2004.

[7] J. Haas and C. Péró, "Mesozoic evolution of the Tisza Mega-unit," *International Journal of Earth Sciences*, vol. 93, no. 2, pp. 297–313, 2004.

[8] J. F. von Raumer, G. M. Stampfli, and F. Bussy, "Gondwana-derived microcontinents – the constituents of the Variscan and Alpine collisional orogens," *Tectonophysics*, vol. 365, no. 1-4, pp. 7–22, 2003.

[9] G. Tari, "The palinspastic position of Tisia(Tisza) in the Alpine realm: a view from the outside of the Pannonian Basin," in *Tisia Conference*, V. Dályay and M. Sámson, Eds., pp. 29–32, Molnár Printing and Publishing, Pécs, 2015.

[10] G. Tari and F. Horváth, "Alpine evolution and hydrocarbon geology of the Pannonian Basin: an overview," in *The Carpathians and their Foreland: Geology and Hydrocarbon Resources, AAPG Memoir, vol. 84*, J. Golonka and F. Picha, Eds., pp. 605–618, AAPG (The American Association of Petroleum Geologists), 2006.

[11] G. Wessely, "Mesozoic and Tertiary evolution of the Alpine-Carpathian foreland in eastern Austria," *Tectonophysics*, vol. 137, no. 1-4, pp. 45–59, 1987.

[12] G. Tari, O. Dicea, J. Faulkerson et al., "Cimmerian and Alpine stratigraphy and structural evolution of the Moesian Platform (Romania/Bulgaria)," in *Regional and Petroleum Geology of the Black Sea and Surrounding Regions. AAPG Memoir, vol.*

68, A. G. Robinson, Ed., pp. 63–90, AAPG (The American Association of Petroleum Geologists), 1997.

[13] G. Tari and P. Strauss, "Examples of the Jurassic Gresten facies from Austria, Romania and Bulgaria: a comparison with the equivalent facies unit in Tisia(Tisza)," in *Tisia Conference*, V. Dálya and M. Sámson, Eds., pp. 42–45, Molnár Printing and Publishing, Pécs, 2015.

[14] E. Pozsgai, S. Józsa, I. Dunkl et al., "Provenance of the Upper Triassic siliciclastics of the Mecsek Mountains and Villány Hills (Pannonian Basin, Hungary): constraints to the Early Mesozoic paleogeography of the Tisza Megaunit," *International Journal of Earth Sciences*, vol. 106, no. 6, pp. 2005–2024, 2017.

[15] P. D. Bons, M. A. Elburg, and E. Gomez-Rivas, "A review of the formation of tectonic veins and their microstructures," *Journal of Structural Geology*, vol. 43, pp. 33–62, 2012.

[16] K. Fintor, F. Schubert, and T. M. Tóth, "Hiperszalin paleofluidum áramlás nyomai a Baksai Komplexum repedésrendszerében," *Földtani Közlöny*, vol. 138, no. 3, pp. 257–278, 2008.

[17] K. Fintor, T. M. Tóth, and F. Schubert, "A Baksai Komplexum posztmetamorf fluidum evolúciója," in *Magmás és metamorf képződmények a Tiszai Egységben*, T. M. Tóth, Ed., pp. 245–258, Geolitera, Szeged, 2009.

[18] K. Fintor, T. M. Tóth, and F. Schubert, "Near vein metasomatism along propylitic veins in the Baksa Gneiss Complex, Pannonian Basin, Hungary," *Geologia Croatica*, vol. 63, pp. 75–91, 2010.

[19] K. Fintor, T. M. Tóth, and F. Schubert, "Hydrothermal palaeofluid circulation in the fracture network of the Baksa Gneiss Complex of SW Pannonian Basin, Hungary," *Geofluids*, vol. 11, no. 2, pp. 144–165, 2011.

[20] A. Varga, G. Szakmány, S. Józsa, and Z. Máthé, "A nyugat-mecseki alsó-miocén konglomerátum karbon homokkő kavicsainak és a Tésenyi Homokkő Formáció képződményeinek petrográfiai és geokémiai összehasonlítása," *Földtani Közlöny*, vol. 131, no. 1–2, pp. 11–36, 2001.

[21] A. R. Varga, G. Szakmány, S. Józsa, and Z. Máthé, "Petrology and geochemistry of Upper Carboniferous siliciclastic rocks (Téseny Sandstone Formation) from the Slavonian–Drava Unit (Tisza Megaunit, S Hungary) – summarized results," *Acta Geologica Hungarica*, vol. 46, no. 1, pp. 95–113, 2003.

[22] A. Varga and G. Szakmány, "Geochemistry and provenance of the upper carboniferous sandstones from borehole Diósviszló–3 (Téseny Sandstone Formation, SW Hungary)," *Acta Mineralogica-Petrographica, Szeged*, vol. 45, no. 2, pp. 7–14, 2004.

[23] A. Varga, B. Raucsik, and G. Szakmány, "A Siklósbodony Sb–1 mélyfúrás feltételezett karbon–perm határképződményeinek ásványtani, kőzettani és geokémiai jellemzői," *Földtani Közlöny*, vol. 134, no. 3, pp. 321–343, 2004.

[24] A. Varga, G. Szakmány, T. Árgyelán, S. Józsa, B. Raucsik, and Z. Máthé, "Complex examination of the Upper Paleozoic siliciclastic rocks from southern Transdanubia, SW Hungary – mineralogical, petrographic, and geochemical study," in *Sedimentary Provenance and Petrogenesis: Perspectives from Petrography and Geochemistry, Geological Society of America Special Paper 420*, J. Arribas, S. Critelli, and M. J. Johnsson, Eds., pp. 221–240, The Geological Society of America, 2007.

[25] A. Varga, B. Raucsik, and G. Szakmány, "On possible origin of background contents of heavy metals and metalloids in the subsurface Pennsylvanian Téseny metasandstones, SW Hungary," *Carpathian Journal of Earth and Environmental Sciences*, vol. 7, no. 3, pp. 211–218, 2012.

[26] A. Vozárová, F. Ebner, S. Kovács et al., "Late Variscan (Carboniferous to Permian) environments in the Circum Pannonian Region," *Geologica Carpathica*, vol. 60, no. 1, pp. 71–104, 2009.

[27] J. Vozár, F. Ebner, A. Vozárová et al., *Variscan and Alpine Terranes of the Circum-Pannonian Region*, Slovak Academy of Sciences, Geological Institute, Bratislava, 2010.

[28] M. Szemerédi, A. Varga, R. Lukács, and E. Pál-Molnár, "A Gyűrűfűi Riolit Formáció kőzettani vizsgálata a felszíni előfordulások alapján (Nyugati-Mecsek)," *Földtani Közlöny*, vol. 146, no. 4, pp. 335–354, 2016.

[29] Á. Jámbor, *Karbon képződmények a Mecsek és a Villányi hegység közötti területen*, MÁFI Évi jelentés 1967-ről, 1969.

[30] Á. Jámbor, "A Tiszai nagyszerkezeti egység karbon üledékes képződményei rétegtanának ismertetése," in *Magyarország geológiai képződményeinek rétegtana*, I. Bérczi and Á. Jámbor, Eds., pp. 173–185, Budapest, MOL Rt., MÁFI, 1998.

[31] R. Hetényi and L. Ravaszné Baranyai, *A baranyai antracittelepes felsőkarbon összlet a Siklósbodony 1. és a Bogádmindszent 1. sz. fúrás tükrében*, MÁFI Évi jelentése 1973-ról, 1976.

[32] P. D. Bons, "The formation of veins and their microstructures," in *Stress, Strain and Structure, A Volume in Honour of W D Means, Journal of the Virtual Explorer, Electronic Edition*, M. W. Jessell and J. L. Urai, Eds., Win Means' Publications, 2000.

[33] D. L. Whitney and B. W. Evans, "Abbreviations for names of rock-forming minerals," *American Mineralogist*, vol. 95, no. 1, pp. 185–187, 2010.

[34] R. H. Goldstein and T. J. Reynolds, "Systematics of fluid inclusions in diagenetic minerals," *SEMP Short Course*, vol. 31, 1994.

[35] L. W. Diamond, "Systematics of H_2O inclusions," in *Fluid Inclusions: Analysis and Interpretation, vol. 32*, I. Samson, A. Anderson, and D. Marshall, Eds., pp. 55–77, Mineralogical Association of Canada, Vancouver, 2003.

[36] R. J. Bakker, "Package _FLUIDS_ 1\. Computer programs for analysis of fluid inclusion data and for modelling bulk fluid properties," *Chemical Geology*, vol. 194, no. 1-3, pp. 3–23, 2003.

[37] R. J. Bakker, *Computer Package FLUIDS, Version 2: A New Jacket and Improvements*, PACROFI IX, Reston, VA, USA, 2008.

[38] M. Steele-MacInnis, R. J. Bodnar, and J. Naden, "Numerical model to determine the composition of H_2O-NaCl-$CaCl_2$ fluid inclusions based on microthermometric and microanalytical data," *Geochimica et Cosmochimica Acta*, vol. 75, no. 1, pp. 21–40, 2011.

[39] Y. G. Zhang and J. D. Frantz, "Determination of the homogenization temperatures and densities of supercritical fluids in the system $NaClKClCaCl_2H_2O$ using synthetic fluid inclusions," *Chemical Geology*, vol. 64, no. 3-4, pp. 335–350, 1987.

[40] B. S. Krumgalz, R. Pogorelsky, and K. S. Pitzer, "Volumetric Properties of Single Aqueous Electrolytes from Zero to Saturation Concentration at 298.15°K Represented by Pitzer's Ion-Interaction Equations," *Journal of Physical and Chemical Reference Data*, vol. 25, no. 2, pp. 663–689, 1996.

[41] T. P. Mernagh and A. R. Wilde, "The use of the laser Raman microprobe for the determination of salinity in fluid inclusions," *Geochimica et Cosmochimica Acta*, vol. 53, no. 4, pp. 765–771, 1989.

[42] R. J. Bakker, "Raman spectra of fluid and crystal mixtures in the systems H_2O, H_2O–NaCl and H_2O–$MgCl_2$ at low temperatures: applications to fluid-inclusion research," *The Canadian Mineralogist*, vol. 42, no. 5, pp. 1283–1314, 2004.

[43] R. T. Downs, "The RRUFF Project: an integrated study of the chemistry, crystallography, Raman and infrared spectroscopy of minerals," in *Program and Abstracts of the 19th General Meeting of the International Mineralogical Association in Kobe*, Japan, 2006.

[44] N. Rividi, M. van Zuilen, P. Philippot, B. Ménez, G. Godard, and E. Poidatz, "Calibration of carbonate composition using micro-Raman analysis: application to planetary surface exploration," *Astrobiology*, vol. 10, no. 3, pp. 293–309, 2010.

[45] Y. F. Zheng, "Oxygen isotope fractionation in carbonate and sulfate minerals," *Geochemical Journal*, vol. 33, no. 2, pp. 109–126, 1999.

[46] C. Hilgers and J. L. Urai, "On the arrangement of solid inclusions in fibrous veins and the role of the crack-seal mechanism," *Journal of Structural Geology*, vol. 27, no. 3, pp. 481–494, 2005.

[47] N. Rodrigues, P. R. Cobbold, H. Loseth, and G. Ruffet, "Widespread bedding-parallel veins of fibrous calcite ('beef') in a mature source rock (Vaca Muerta Fm, Neuquén Basin, Argentina): evidence for overpressure and horizontal compression," *Journal of the Geological Society, London*, vol. 166, no. 4, pp. 695–709, 2009.

[48] G. Lelkes-Felvári, R. Schuster, W. Frank, and R. Sassi, "Metamorphic history of the Algyő High (Tisza Mega-unit, basement of Great Hungarian Plain) - a counterpart of crystalline units of the Koralpe-Wölz nappe system (Austroalpine, Eastern Alps)," *Acta Geologica Hungarica*, vol. 48, no. 4, pp. 371–394, 2005.

[49] I. Garaguly, B. Raucsik, A. Varga, and F. Schubert, "Középsőtriász dolomitok képződésének története és töréses deformációja a Szegedi-medence területén," *Földtani Közlöny*, vol. 147, no. 1, pp. 39–60, 2017.

[50] I. Garaguly, A. Varga, B. Raucsik, F. Schubert, G. Czuppon, and R. Frei, "Pervasive early diagenetic dolomitization, subsequent hydrothermal alteration, and late stage hydrocarbon accumulation in a Middle Triassic carbonate sequence (Szeged Basin, SE Hungary)," *Marine and Petroleum Geology*, vol. 98, pp. 270–290, 2018.

[51] N. Papp, A. Varga, E. Mészáros, and B. Raucsik, "A dorozsmai márvány (Tiszai-főegység) kőzettani újravizsgálata: deformáció és fluidum hatása a mikroszerkezet fejlődésére," *Földtani Közlöny*, vol. 147, no. 4, pp. 337–356, 2018.

[52] D. Jamičić, "Strukturni sklop metamorfnih stijena Krndije i južnih padina Papuka," *Geološki vjesnik*, vol. 36, pp. 51–72, 1983.

[53] J. Pamić and I. Jurković, "Paleozoic tectonostratigraphic units of the northwest and central Dinarides and the adjoining South Tisia," *International Journal of Earth Sciences*, vol. 91, no. 3, pp. 538–554, 2002.

[54] V. Biševac, E. Krenn, F. Finger, B. Luzar-Oberiter, and D. Balen, "Provenance of Paleozoic very low- to low-grade metasedimentary rocks of South Tisia (Slavonian Mountains, Radlovac Complex, Croatia)," *Geologica Carpathica*, vol. 64, no. 1, pp. 3–22, 2013.

[55] G. Jerinić, J. Pamić, J. Sremac, and D. Španić, "Palynological and organic-petrographic data on very low- and low-grade metamorphic rocks in the Slavonian Mountains (Northern Croatia)," *Geologia Croatica*, vol. 47, no. 2, pp. 149–155, 1994.

[56] M. Brkić, D. Jamičić, and N. Pantić, "Karbonske naslage u Papuku (Sjeveroistočna Hrvatska)," *Geološki vjesnik*, vol. 27, pp. 53–58, 1974.

[57] J. Fülöp, *Magyarország geológiája, Paleozoikum II*, Akadémiai Kiadó, Budapest, 1994.

[58] V. Biševac, D. Balen, D. Tibljaš, and D. Španić, "Preliminary results on degree of thermal alteration recorded in the eastern part of Mt. Papuk, Slavonia, Croatia," *Geologia Croatica*, vol. 62, no. 1, pp. 63–72, 2009.

[59] V. Biševac, K. Balogh, D. Balen, and D. Tibljaš, "Eoalpine (Cretaceous) very low- to low-grade metamorphism recorded on the illite-muscovite-rich fraction of metasediments from South Tisia (eastern Mt Papuk, Croatia)," *Geologica Carpathica*, vol. 61, no. 6, pp. 469–481, 2010.

[60] M. R. Bathia and K. A. W. Crook, "Trace elements characteristics of graywackes and tectonic setting discriminations of sedimentary basins," *Contribution to Mineralogy and Petrology*, vol. 92, pp. 181–193, 1986.

[61] T. Szederkényi, "A mecseki ópaleozoos-prekambriumi alapszelvények komplex földtani feldolgozása," in *Manuscript, Hungarian Geological Survey*, p. 139, JATE, Szeged, 1979.

[62] T. Tarnai, "Ore minerals from the key section of the Baksa Complex (W Baranya Hills, Hungary)," *Acta Mineralogica-Petrographica, Szeged*, vol. 38, pp. 119–133, 1997.

[63] T. Tarnai, "Mineralogical-petrological study on ore vein penetrated by the key-borehole Baksa No. 2 SE Transdanubia, Hungary," *Acta Mineralogica-Petrographica, Szeged*, vol. 39, pp. 21–34, 1998.

[64] T. Fehér and A. Molnár, "Petrographic study of the Mórágy-type granitoid and the Cserdi Conglomerate at Nyugotszenterzsébet (Mecsek Mts., South Hungary)," *Acta Mineralogica-Petrographica, Szeged*, vol. 30, pp. 93–101, 1989.

[65] J. Vince, K. G. Sólymos, Z. Ditrói-Puskás, and L. Kósa, "Mikroteléres, -eres uránérc a nyugat-mecseki gránitban," *Földtani Közlöny*, vol. 141, no. 4, pp. 325–339, 2011.

[66] B. Kříbek, K. Žák, P. Dobeš et al., "The Rožná uranium deposit (Bohemian Massif, Czech Republic): shear zone-hosted, late Variscan and post-Variscan hydrothermal mineralization," *Mineralium Deposita*, vol. 44, no. 1, article 188, pp. 99–128, 2009.

[67] H. J. Behr and J. Gerler, "Inclusions of sedimentary brines in post-Variscan mineralizations in the Federal Republic of Germany – A study by neutron activation analysis," *Chemical Geology*, vol. 61, no. 1-4, pp. 65–77, 1987.

[68] H. J. Behr, E. E. Horn, K. Frentzel-Beyme, and C. Reutel, "Fluid inclusion characteristics of the Variscan and post-Variscan mineralizing fluids in the Federal Republic of Germany," *Chemical Geology*, vol. 61, no. 1-4, pp. 273–285, 1987.

[69] G. Lelkes-Felvári and W. Frank, "Geochronology of the metamorphic basement, Transdanubian part of the Tisza Mega-Unit," *Acta Geologica Hungarica*, vol. 49, no. 3, pp. 189–206, 2006.

[70] A. Varga, G. Újvári, and J. Kovács, "Cirkon egykristály U-Pb korok a danitzpusztai pannóniai homokból: közvetett bizonyítékok az aljzatot alkotó metamorfitok kevert prevariszkuszi protolitjaira," *Földtani Közlöny*, vol. 142, no. 1, pp. 95–98, 2012.

[71] H. Lapierre, C. Basile, T. Berly, and E. Canard, "Potassic late orogenic Stephanian volcanism in the Southwest French Massif Central (Decazeville, Figeac, Lacapelle-Marival basins): an

example for mantle metasomatism along strike-slip faults?," *Bulletin de la Societe Geologique de France*, vol. 179, no. 5, pp. 491–502, 2008.

[72] P. Árkai, K. Balogh, A. Demény, I. Fórizs, G. Nagy, and Z. Máthé, "Composition, diagenetic and post-diagenetic alterations of a possible radioactive waste repository site: the Boda Albitic Claystone Formation, southern Hungary," *Acta Geologica Hungarica*, vol. 43, pp. 351–378, 2000.

[73] A. Varga, G. Szakmány, B. Raucsik, and Z. Máthé, "Chemical composition, provenance and early diagenetic processes of playa lake deposits from the Boda Siltstone Formation (Upper Permian), SW Hungary," *Acta Geologica Hungarica*, vol. 48, pp. 49–68, 2005.

[74] G. Konrád, K. Sebe, A. Halász, and E. Babinszki, "Sedimentology of a Permian playa lake: the Boda Claystone Formation, Hungary," *Geologos*, vol. 16, no. 1, pp. 27–41, 2010.

[75] Z. Máthé and A. Varga, ""Ízesítő" a permi Bodai Agyagkő Formáció őskörnyezeti rekonstrukciójához: kősó utáni pszeudomorfózák a BAT–4 fúrás agyagkőmintáiban," *Földtani Közlöny*, vol. 142, pp. 201–204, 2012.

[76] G. Dabi, Z. Siklósy, F. Schubert, B. Bajnóczi, and T. M. Tóth, "The relevance of vein texture in understanding the past hydraulic behaviour of a crystalline rock mass: reconstruction of the palaeohydrology of the Mecsekalja Zone, South Hungary," *Geofluids*, vol. 11, no. 3, pp. 309–327, 2011.

[77] G. Dabi, F. Tóth, and F. Schubert, "Preliminary fluid inclusion microthermometry results from secondary inclusion planes crosscutting a metamorphic quartz lens from the Mecsekalja Zone metamorphic complex," *Central European Geology*, vol. 60, no. 2, pp. 152–172, 2017.

[78] J. N. Rubin, C. D. Henry, and J. G. Price, "The mobility of zirconium and other "immobile" elements during hydrothermal alteration," *Chemical Geology*, vol. 110, no. 1-3, pp. 29–47, 1993.

[79] M. René, "Rare-earth, yttrium and zirconium mobility associated with the uranium mineralisation at Okrouhlá Radouň, Bohemian Massif, Czech Republic," *European Journal of Mineralogy*, vol. 27, no. 1, pp. 57–70, 2015.

[80] C. Ballouard, M. Poujol, P. Boulvais et al., "Magmatic and hydrothermal behavior of uranium in syntectonic leucogranites: The uranium mineralization associated with the Hercynian Guerande granite (Armorican Massif, France)," *Ore Geology Reviews*, vol. 80, pp. 309–331, 2017.

[81] V. Ziegler and J. Dardel, "Uranium deposits in Europe," in *Uranium geochemistry, mineralogy, geology, exploration and resources*, B. Vivo, Ed., pp. 140–161, Springer, Dordrecht, 1984.

[82] H. Dill, "The polymetallic and monotonous uranium parageneses – a contribution of the position of endogenous uranium mineralization at the western edge of the Bohemian Massif," *Neues Jahrbuch für Mineralogie - Monatshefte*, vol. 4, pp. 184–192, 1985.

[83] K. Žák, P. Dobeš, B. Kříbek, M. Pudilová, A. Hájek, and D. Holeczy, "Evolution of fluid types at the Rožná uranium deposit, Czech Republic. Stable isotope and fluid inclusion study," in *Mineral deposits at the beginning of the 21st century*, J. Piestrzyński, Ed., pp. 109–113, Balkema, Lisse, 2001.

[84] M. René, "Geochemical constraints of hydrothermal alterations of two-mica granites of the Moldanubian Batholith at the Okrouhlá Radouň uranium deposit," *Acta Geodynamica et Geomaterialia*, vol. 2, no. 4, pp. 63–79, 2005.

[85] M. René, "Alteration of granitoids and crystalline rocks and uranium mineralisation in the Bor pluton area, Bohemian Massif, Czech Republic," *Ore Geology Reviews*, vol. 81, pp. 188–200, 2017.

[86] Z. Dolníček, M. René, S. Hermannová, and W. Prochaska, "Origin of the Okrouhlá Radouň episyenite-hosted uranium deposit, Bohemian Massif, Czech Republic: fluid inclusion and stable isotope constraints," *Mineralium Deposita*, vol. 49, no. 4, pp. 409–425, 2014.

[87] P. Horváth, G. Kovács, and G. Szakmány, "Eclogite and garnet amphibolite pebbles from Miocene conglomerates (Pannonian Basin, Hungary): implications for the Variscan metamorphic evolution of the Tisza Megaunit," *Geologica Carpathica*, vol. 54, no. 6, pp. 355–366, 2003.

[88] J. F. von Raumer, F. Finger, P. Veselá, and G. M. Stampfli, "Durbachites-Vaugnerites – a geodynamic marker in the central European Variscan orogen," *Terra Nova*, vol. 26, no. 2, pp. 85–95, 2014.

[89] F. Finger, A. Gerdes, V. Janoušek, M. René, and G. Riegler, "Resolving the Variscan evolution of the Moldanubian sector of the Bohemian Massif: the significance of the Bavarian and the Moravo-Moldanubian tectonometamorphic phases," *Journal of Geosciences*, vol. 52, no. 1–2, pp. 9–28, 2007.

[90] V. Janoušek and F. V. Holub, "The causal link between HP-HT metamorphism and ultrapotassic magmatism in collisional orogens: case study from the Moldanubian Zone of the Bohemian Massif," *Proceedings of the Geologists' Association*, vol. 118, no. 1, pp. 75–86, 2007.

[91] L. Ravasz-Baranyai, "Eclogite from the Mecsek Mountains, Hungary," *Acta Geologica Academiae Scientiarum Hungaricae*, vol. 13, pp. 315–322, 1969.

[92] T. M. Tóth, "Geochemistry of the Görcsöny Ridge amphibolites (Tisza Unit, SW Hungary) and its geodynamic consequences," *Geologia Croatica*, vol. 67, no. 1, pp. 17–32, 2014.

[93] A. Kis, T. G. Weiszburg, I. Dunkl, F. Koller, T. Váczi, and Gy. Buda, "Comparative U-Pb geochronology on zircon crystals from Mórágy, Hungary," *Meeting of Young Geoscientists, Kaposvár*, pp. 69-70, 2017.

[94] T. Szederkényi, "Metamorphic formations and their correlation in the Hungarian part of the Tisia megaunit (Tisia Composite Terrane)," *Acta Mineralogica-Petrographica, Szeged*, vol. 37, pp. 143–160, 1996.

[95] G. Kovács, B. G. Radovics, and T. M. Tóth, "Petrologic comparison of the Gyód and Helesfa serpentinite bodies (Tisia Mega Unit, SW Hungary)," *Journal of Geosciences*, vol. 61, pp. 255–263, 2016.